

Domain Adaptation for Time Series Under Feature and Label Shifts

Huan He¹ Owen Queen¹ Teddy Koker² Consuelo Cuevas² Theodoros Tsiligkaridis² Marinka Zitnik¹

Abstract

The transfer of models trained on labeled datasets in a source domain to unlabeled target domains is made possible by unsupervised domain adaptation (UDA). However, when dealing with complex time series models, the transferability becomes challenging due to the dynamic temporal structure that varies between domains, resulting in feature shifts and gaps in the time and frequency representations. Furthermore, tasks in the source and target domains can have vastly different label distributions, making it difficult for UDA to mitigate label shifts and recognize labels that only exist in the target domain. We present RAINCOAT, the first model for both closed-set and universal DA on complex time series. RAINCOAT addresses feature and label shifts by considering both temporal and frequency features, aligning them across domains, and correcting for misalignments to facilitate the detection of private labels. Additionally, RAINCOAT improves transferability by identifying label shifts in target domains. Our experiments with 5 datasets and 13 state-of-the-art UDA methods demonstrate that RAINCOAT can achieve an improvement in performance of up to 16.33%, and can effectively handle both closed-set and universal adaptation.

1. Introduction

Neural networks have demonstrated impressive performance on time series datasets (Ravuri et al., 2021; Lundberg et al., 2018). However, their performance deteriorates rapidly under domain shifts, making it challenging to deploy these models in real-world scenarios (Zhang et al., 2022a;b). Domain shifts occur when the test distribution is not identical to the training data, even though it is often related (Koh et al.,

¹Department of Biomedical Informatics, Harvard Medical School ²Artificial Intelligence Technology, MIT Lincoln Laboratory. Correspondence to: Huan He, Theodoros Tsiligkaridis, Marinka Zitnik <huan_he@hms.harvard.edu, ttsili@ll.mit.edu, marinka@hms.harvard.edu>.

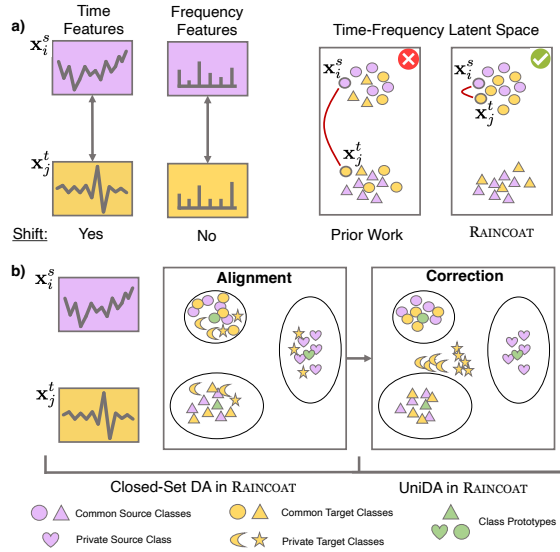


Figure 1. **a)** RAINCOAT captures domain-invariant frequency features under time feature shift. **b)** For Closed-Set DA, RAINCOAT aligns source and target domains for greater generalization. For Universal DA, the correction step prioritizes target-specific features to detect private target classes.

2021; Luo et al., 2018; Zhang et al., 2013), meaning that latent representations do not generalize to test datasets drawn from different underlying distributions, even if the differences between these distributions are minor. To overcome these challenges, domain adaptation (DA) has emerged as a set of techniques that allow adaptation to new target domains and reduce bias by leveraging unlabeled data in target domains (Ganin et al., 2016; Long et al., 2015).

Training models that can adapt to domain shifts is crucial for robust, real-world deployment. For instance, for healthcare time series, data collection methods vary widely across different clinical sites (domains) (Zhang et al., 2022c), leading to shifts in the underlying features and labels. It is preferable to train a model on a diverse dataset collected from multiple clinics rather than training and applying individual models on smaller, single-domain datasets for each clinic. Additionally, training a model that can detect unknown classes in test data, such as patients with rare diseases (Alsentzer et al., 2022), is advantageous for real-world implementation among end-users, such as clinicians (Tonekaboni et al.,

2019). Endowing learning systems with DA capabilities can increase their reliability and expand applicability across downstream tasks.

DA is a highly complex problem due to several factors. First, models trained for robustness to domain shifts must learn highly generalizable features; however, neural networks trained using standard practices can rely on spurious correlations created by non-causal data artifacts (Geirhos et al., 2020; DeGrave et al., 2021), hindering their ability to transfer across domains. Additionally, shifts in label distributions across domains may result in *private labels*, i.e., classes that exist in the target domain but not in the source domain (Lipton et al., 2018). In unsupervised DA, a model must generalize across domains when labels from the target domain are not available during training (Long et al., 2018a; Kang et al., 2019a). Therefore, DA methods must be able to identify when a private label is encountered in the target domain without any prior supervision on detecting these unknown labels (You et al., 2019; Fu et al., 2020). Yet, that is not possible by techniques that rely on training samples that simulate predicting unknown labels. This highlights the need for time series DA methods that 1) produce *generalizable representations robust to feature and label shifts*, and 2) expand the scope of existing DA methods by supporting both *closed-set* and *universal* DA.

DA becomes even more challenging when applied to time series data. Domain shifts can occur in both the time and frequency features of time series, which can create a shift that highly perturbs time features while frequency features are relatively unchanged, or vice versa (Fig. 1a). Previous time series DA methods fail to explicitly model frequency features, which can lead to catastrophic negative transfer. Additionally, the area of universal DA for time series, when no assumptions are made about the overlap between labels in the source and target domains, is an unexplored area of research (Fig. 1b). There is a crucial need for robust methods with inductive biases specific to time series.

Present Work. We introduce RAINCOAT (fRrequency-augmented AlIgN-then-Correct for doMain Adaptation for Time series)¹, a novel domain adaptation method for time series data that can handle both feature and label shifts (as shown in Fig. 1). Our method is the first to address both closed-set and universal domain adaptation for time series and has the unique capability of handling feature and label shifts. To achieve this, we first use time and frequency-based encoders to learn time series representations, motivated by inductive bias that domain shifts can occur via both time or frequency feature shifts. Next, we propose the use of Sinkhorn divergence for source-target feature alignment, and provide both empirical evidence

and theoretical justification for its superiority over other popular divergence measures. Finally, we introduce an “align-then-correct” procedure for universal DA, which first aligns the source and target domains, retrains the encoder on the target domain to correct misalignments, and then measures the difference between the aligned and corrected representations of target samples to detect unknown target classes (as shown in Fig. 2). We evaluate RAINCOAT on five time series datasets from various modalities, including human activity recognition, mechanical fault detection, and electroencephalogram prediction. Our method outperforms strong baselines by up to 9.0% for closed-set DA and 16.33% for universal DA. The source code are available at <https://github.com/mims-harvard/Raincoat>.

2. Related Work

General Domain Adaptation. General domain adaptation (DA), leveraging labeled source domain to predict labels on the unlabeled target domain, has a wide range of applications (Ganin and Lempitsky, 2015; Sener et al., 2016; Zhang et al., 2018; Perone et al., 2019; Ramponi and Plank, 2020). We organize DA methods into three categories: 1) *Adversarial training*: A domain discriminator is optimized to distinguish source and target domains, while a deep classification model learns transferable features indistinguishable by the domain discriminator (Hoffman et al., 2015; Tzeng et al., 2017; Motiian et al., 2017; Long et al., 2018a; Hoffman et al., 2018). 2) *Statistical divergence*: These approaches aim to extract domain invariant features by minimizing domain discrepancy in a latent feature space. Widely used measures include MMD (Rozantsev et al., 2016), correlation alignment (CORAL) (Sun and Saenko, 2016), contrastive domain discrepancy (CDD) (Kang et al., 2019a), optimal transport distance (Courty et al., 2017; Redko et al., 2019), and graph matching loss (Yan et al., 2016; Das and Lee, 2018). 3) *Self-supervision*: These general DA approaches incorporate auxiliary self-supervision training tasks. These methods learn domain-invariant features through a pretext learning task, such as data augmentation and reconstruction, for which a target objective can be computed without supervision. Contrastive methods capture the semantic information of the samples by maximizing the lower bound of the mutual information between two augmented views (Kang et al., 2019b; Singh, 2021; Tang et al., 2021). In addition, reconstruction-based methods achieve alignment by carrying out source domain classification and reconstruction of target domain data or both source and target domain data (Ghifary et al., 2016; Jhuo et al., 2012). More discussion can be founded in existing review papers focusing on domain adaptation (Ramponi and Plank, 2020; Liu et al., 2022). RAINCOAT sits in the category of both 2 and 3.

Domain Adaptation for Time Series. While in light of

¹Project Website: <https://zitniklab.hms.harvard.edu/projects/Raincoat/>

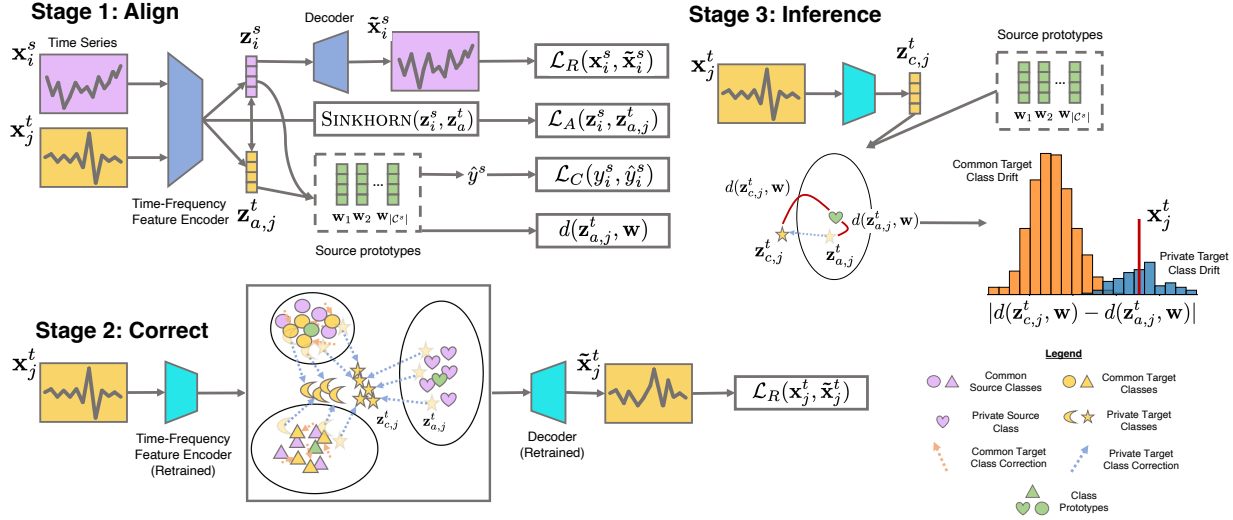


Figure 2. Illustration of the RAINCOAT method for time series DA. Details provided in-text.

successes in computer vision, limited methods have focused on adaptation approaches for time series data. To date, few DA methods are specifically designed for time series. 1) *Adversarial training*: VRADA (Purushotham et al., 2017) builds upon a variational recurrent neural network (VRNN) and trains adversarially to capture complex temporal relationships that are domain-invariant. CoDATS (Wilson et al., 2020) builds upon VRADA but uses a convolutional neural network for the feature extractor. 2) *Statistical divergence*: SASA (Cai et al., 2021) aligns the condition distribution of the time series data by minimizing the discrepancy of the associative structure of time series variables between domains. AdvSKM (Liu and Xue, 2021a) and (Ott et al., 2022) are metric-based methods that align two domains by considering statistic divergence. 3) *Self-supervision*: DAF (Jin et al., 2022) extracts domain-invariant and domain-specific features to perform forecasts for source and target domains through a shared attention module with a reconstruction task. CLUDA (Ozyurt et al., 2022) and CLADA (Wilson et al., 2021) are two contrastive DA methods that use augmentations to extract domain invariant and contextual features for prediction. However, the above methods align features without considering the potential gap between labels from both domains. Moreover, they focus on aligning only time features while ignoring the implicit frequency feature shift (Fig. 1a). In contrast, RAINCOAT considers the frequency feature shift to mitigate both feature and label shift in DA.

Universal Domain Adaptation. Prevailing DA methods assume all labels in the target domain are also available in the source domain. This assumption, known as closed-set DA, posits that the domain gap is driven by feature shift (as opposed to label shift). In practice, however, the label overlap between the two domains is unknown. Thus, it is

more practical to assume the domain gap can be caused by both feature and label shifts. In contrast to closed-set DA, universal domain adaptation (UniDA) (You et al., 2019) can account for label shift. UniDA categorizes target samples into either common labels (present in both source and target domains) or private labels (present in target domain only). UAN (You et al., 2019), CMU (Fu et al., 2020), and TNT (Chen et al., 2022a) use sample-level uncertainty criteria to measure domain transferability. Samples with lower uncertainty are preferentially selected for adversarial adaptation. However, most UniDA methods detect common samples using sample-level criteria, requiring users to specify the threshold to recognize private labels. Moreover, over-reliance on source supervision neglects discriminative representation in the target domain. DANCE (Saito et al., 2020) uses self-supervised neighborhood clustering to learn features to discriminate private labels. Similarly, DCC (Li et al., 2021a) enumerates cluster numbers of the target domain to obtain optimal cross-domain consensus clusters as common classes. Still, the consensus clusters are not robust enough due to challenging cluster assignments. MATHS (Chen et al., 2022b) detects private labels via mutual nearest-neighbor contrastive learning. In contrast, UniOT (Chang et al., 2022) uses optimal transport to detect common samples and produce representations for samples in the target domain. However, these methods use a feature encoder shared across both domains even though the source and target domains are shifted. In addition, most require fine-tuned thresholds to recognize private labels. RAINCOAT specifies target-specific feature encoders that preserve the semantic meaning of the target domain and makes inference without depending on a user-specified threshold.

3. Problem Setup and Formulation

Notation. We are given a dataset $\mathcal{D} = \{(\mathbf{x}_i, y_i)\}_{i=1}^n$ of n multivariate time series samples where i -th sample $\mathbf{x}_i \in \mathbb{R}^{T \times d}$ contains readouts of d sensors over T time points. Without loss of generality, we consider regular time series — RAINCOAT can be used with techniques, such as Raindrop (Zhang et al., 2022b) to handle irregular time series. We use \mathbf{x}_i to denote a time series (both univariate and multivariate). Each label y_i in \mathcal{D} belongs to the label set \mathcal{C} , i.e., $y_i \in \mathcal{C}$. We use $\mathcal{D}^s = \{(\mathbf{x}_i^s, y_i^s)\}_{i=1}^{n_s}$ to denote the source domain dataset with n_s labeled samples, where \mathbf{x}_i^s is a source domain sample and y_i^s is the associated label. The target domain dataset is unlabeled and denoted as $\mathcal{D}^t = \{(\mathbf{x}_i^t)\}_{i=1}^{n_t}$ with n_t unlabeled samples. Source and target label sets are denoted as \mathcal{C}^s and \mathcal{C}^t , respectively. Zero, one or more labels may be shared between source and target domains, which we denote as $\mathcal{C}^{s,t} = \mathcal{C}^s \cap \mathcal{C}^t$. Source and target domains have their samples drawn from source and target distributions, $\mathcal{D}^s \sim p_s(\mathbf{x}^s, y^s)$ and $\mathcal{D}^t \sim p_t(\mathbf{x}^t, y^t)$.

We consider two types of domain shifts: feature shift and label shift. Feature shift occurs when marginal probability distributions of \mathbf{x} differ, $p_s(\mathbf{x}) \neq p_t(\mathbf{x})$, while conditional probability distributions remain constant across domains, $p_s(y|\mathbf{x}) = p_t(y|\mathbf{x})$ (Zhang et al., 2013). Label shift occurs when marginal probability distributions of y differ, $p_s(y) \neq p_t(y)$. Feature shifts may occur in time series due to, for example, differences in sensor measurement setup or length of samples. A unique property of time series is that feature shifts may occur in either the time or frequency spectrum. The importance of modeling shifts in both the time and frequency spectrum is discussed in later sections. Label shift may occur as either a change in the proportion of classes in either domain or as a categorical shift: both domains might contain different classes in their label sets.

Problem 3.1 (Closed-set Domain Adaptation for Time Series Classification). Given are the source and target domain time series datasets, \mathcal{D}^s and \mathcal{D}^t , whose label sets are the same, $\mathcal{C}^s = \mathcal{C}^t$, and target labels y^t are not available at train time. RAINCOAT specifies a strategy to train a classifier f on \mathcal{D}^s such that f generalizes to \mathcal{D}^t , i.e., it minimizes classification risk on \mathcal{D}^t : $\mathbb{E}_{\mathbf{x}_i, y_i \sim \mathcal{D}^t} [\mathcal{L}_C(f(\mathbf{x}_i), y_i)]$, where \mathcal{L}_C is a classification loss function.

In a real-world application, little information may be available on the feature or label distribution of the target domain. Private labels in either the source or target domain may exist, i.e., classes that are present in one domain but absent in the other. Thus, it is desirable to relax the strict assumption of $\mathcal{C}^s = \mathcal{C}^t$ made by Problem 3.1. We denote source private labels as $\bar{\mathcal{C}}^s = \mathcal{C}^s \setminus \mathcal{C}^t$, target private labels as $\bar{\mathcal{C}}^t = \mathcal{C}^t \setminus \mathcal{C}^s$, and labels shared between domains as $\mathcal{C}^{s,t} = \mathcal{C}^s \cap \mathcal{C}^t$. We denote the access of samples in dataset \mathcal{D} belonging to label set \mathcal{C} as $\mathcal{D}[\mathcal{C}]$, e.g., samples in the target domain belonging

to the common label set would be denoted as $\mathcal{D}^t[\mathcal{C}^{s,t}]$. Domains might not have any common labels, $\mathcal{C}^{s,t} = \emptyset$, leading to the definition of universal DA.

Problem 3.2 (Universal Domain Adaptation (UniDA) for Time Series Classification). Given our source and target domain time series datasets, \mathcal{D}^s and \mathcal{D}^t , where target labels y^t are not available at train time. RAINCOAT specifies a strategy to train a classifier f on \mathcal{D}^s such that f generalizes to \mathcal{D}^t , i.e., it minimizes classification risk of a loss function \mathcal{L}_C on samples belonging to $\mathcal{C}^{s,t}$ in \mathcal{D}^t : $\mathbb{E}_{\mathbf{x}_i, y_i \sim \mathcal{D}^t[\mathcal{C}^{s,t}]} [\mathcal{L}_C(f(\mathbf{x}_i), y_i)]$, while identifying samples in *private* target classes, $\mathbf{x}_i \sim \mathcal{D}^t[\bar{\mathcal{C}}^t]$, as *unknown* samples.

4. Preliminaries

Discrete Fourier Transform. Given a series sample \mathbf{x} with d channels and T time points, it is transformed to the frequency space by applying the 1-dim DFT of length T to each channel and then transforming it back using the 1-dim inverse DFT, defined as:

$$\begin{aligned} \text{Forward DFT : } \mathbf{v}[m] &= \sum_{t=0}^{T-1} \mathbf{x}[t] \cdot e^{-i2\pi \frac{mt}{T}} \\ \text{Inverse DFT : } \mathbf{x}[n] &= \frac{1}{T} \sum_{t=0}^{T-1} \mathbf{v}[m] \cdot e^{i2\pi \frac{mt}{T}} \end{aligned} \quad (1)$$

where T = number of points, n = current point index, m = current frequency index, where $m \in [0, T-1]$. We denote the extracted amplitude and phase as \mathbf{a} and \mathbf{p} respectively:

$$\begin{aligned} \mathbf{a}[m] &= \frac{|\mathbf{v}[m]|}{T} = \frac{\sqrt{\text{Re}(\mathbf{v}[m])^2 + \text{Im}(\mathbf{v}[m])^2}}{T} \\ \mathbf{p}[m] &= \text{atan2}(\text{Im}(\mathbf{v}[m]), \text{Re}(\mathbf{v}[m])) \end{aligned} \quad (2)$$

where $\text{Im}(\mathbf{v}[m])$ and $\text{Re}(\mathbf{v}[m])$ are the imagery and real part of the complex number, atan2 is the two-argument form of arctan.

5. RAINCOAT Approach

We start with an overview of RAINCOAT and proceed with (5.2) time-frequency encoding, (5.3) feature alignment, (5.4) unknown sample detection, and (5.5) training and inference.

5.1. Overview

RAINCOAT is an unsupervised method for closed set and universal domain adaptation in time series, addressing Problems 3.1-3.2. RAINCOAT consists of three modules: a time-frequency encoder G_{TF} , a classifier H , and an auxiliary decoder U_{TF} . Sec. 5.2 describes the encoder G_{TF} , which leverages both time and frequency features. Sec. 5.3 describes how Sinkhorn divergence is a suitable divergence measurement to align the source and target domain because frequency features may not share the same support across both domains. Sec. 5.4 motivates the correction

step for UniDA. Sec. 5.5 describes how RAINCOAT detects potential unknown samples through analysis of pre- and post-correction embeddings. Finally, Sec. 5.6 provides an overview of RAINCOAT models.

5.2. Time-Frequency Feature Encoder

We begin by highlighting the significance of frequency features in UniDA for time series. Although various methods have been proposed to solve the time series UniDA problem under the assumption of feature shift, none of them explicitly address situations where changes in the frequency domain also act as an implicit feature shift. To fill this gap, RAINCOAT encodes both time and frequency features in its latent representations. The source frequency and time features are denoted as $e_{F,i}^s$ and $e_{T,i}^s$, respectively, while the target frequency and time features are represented as $e_{F,i}^t$ and $e_{T,i}^t$. For simplicity, the superscript indicating the source or target domain is omitted in the rest of the text.

Shift of frequency features. We formalize the frequency shift of time series as another type of feature shift. For this purpose, we use the Fourier transform, with the possibility of exploring other options such as wavelets left for future work. A time series \mathbf{x}_i can be represented as a combination of sinusoids, each with a specific frequency, amplitude, and phase, as explained in Sec. 4. If the conditional distributions of the labels with respect to the frequency features are equal ($p_s(y|DFT(\mathbf{x}^s)) = p_t(y|DFT(\mathbf{x}^t))$), but the domains have different frequency features ($p(DFT(\mathbf{x}^s)) \neq p(DFT(\mathbf{x}^t))$), then a frequency shift occurs.

Frequency features help with adaptation. Ben-David et al.; Ben-David et al. demonstrated that the performance of DA techniques is bounded by the divergence between the source and target domains, and that a small feature shift is necessary for DA techniques to be effective. However, unsupervised DA methods for time series align only time features ($e_{T,i}^s$ and $e_{T,i}^t$), leading to sub-optimal performance when the time feature shift is large. By including frequency features in the encoder G_{TF} , we can uncover potential invariant features across domains and improve transferability. For instance, Figure 3 illustrates the sensor readings of walking activity from two different individuals (\mathbf{x}_i^s and \mathbf{x}_i^t) in the WISDM dataset (Kwapisz et al., 2011) and their corresponding Fourier features ($e_{F,i}^s$ and $e_{F,i}^t$). Using only time features would result in poor predictions in the target domain due to a significant time feature shift between \mathbf{x}_i^s and \mathbf{x}_i^t . On the other hand, frequency features from different domains do not exhibit significant feature shifts and thus are domain invariant. This suggests that incorporating frequency features can lead to more accurate predictions in the target domain as DA aims to extract domain-invariant features. For this reason, RAINCOAT uses both time and frequency features in domain alignment.

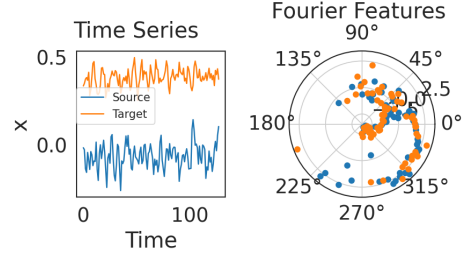


Figure 3. *Left:* averaged sensor readings (one channel) of the walking activity collected from two persons (source and target). *Right:* corresponding polar coordinates of Fourier features. Fourier features are more domain-invariant than time features.

Frequency Feature Encoder. Inspired by Fourier neural operator (FNO) (Li et al., 2021b), RAINCOAT applies convolution on low-frequency modes of the Fourier transform of \mathbf{x}_i . We make two modifications to improve the utility of Fourier convolution for DA: 1) *Prevent Frequency Leakage:* Discrete Fourier Transform considers inputs \mathbf{x}_i to be periodic. Violation of such assumption results in frequency leakage (Harris, 1978). For example, consider a single frequency component input $\mathbf{x}[t] = \cos(2\pi mt)$ with $m = 2\text{Hz}$, which it samples over 1 second, applying DFT outputs only one non-zero frequency bin. But if DFT is applied only on a fraction of $\mathbf{x}[t]$ (0.6 seconds), it may output multiple non-zero frequency bins. The discontinuities at the boundaries of the observation are responsible for such frequency leakage, which is common in time series analysis due to the slicing window preprocessing manner. Specifically, given two window sliced time series \mathbf{x}_i^s and \mathbf{x}_i^t , applying DFT (1) could return perturbed and noisy \mathbf{v}_i^s and \mathbf{v}_i^t which may lead to noisy-biased domain alignment. To prevent aligning on noisy frequency features, RAINCOAT applies a smoothing function (cosine function) before applying DFT. 2) *Consider amplitude \mathbf{a}_i and phase \mathbf{p}_i information:* Instead of using inverse DFT to convert \mathbf{v}_i back to time-space which is an unnecessary step for frequency feature extraction, RAINCOAT extracts the polar coordinates of frequency coefficients to keep both low-level (\mathbf{a}_i) and high-level (\mathbf{p}_i) semantics. The frequency space features e_F is a concatenation $[\mathbf{a}_i; \mathbf{p}_i]$.

Now we summarize how G_{FT} encodes time-frequency feature from \mathbf{x}_i . Define a convolution operator “ $*$ ” and weight matrix \mathbf{B} , the encoder G_F encodes frequency features $e_{F,i}$ by: 1) *Smooth:* $\mathbf{x}_i = \text{Smooth}(\mathbf{x}_i)$, 2) *DFT:* $\mathbf{v}_i = \text{DFT}(\mathbf{x}_i)$, 3) *Convolution:* $\tilde{\mathbf{v}}_i = \mathbf{B} * \mathbf{v}_i$, 4) *Transform:* $\mathbf{a}_i, \mathbf{p}_i \leftarrow \tilde{\mathbf{v}}_i$ (Use Eq. 2), 5) *Extract:* $e_{F,i} = [\mathbf{a}_i; \mathbf{p}_i]$. The time features $e_{T,i}$ can be obtained using any existing time feature encoder, such as CNNs. Finally, the latent representation \mathbf{z}_i is a concatenation of frequency and time features $[e_{F,i}; e_{T,i}]$. Details are in Appendix B.

5.3. Domain Alignment of Time-Frequency Features

Next, we address the question of what is the appropriate metric to align frequency features between \mathbf{e}_F^s and \mathbf{e}_F^t . RAINCOAT represents the frequency features as the amplitude and phase, $\mathbf{e}_{F,i}^s = [\mathbf{a}_i^s; \mathbf{p}_i^s]$, $\mathbf{e}_{F,i}^t = [\mathbf{a}_i^t; \mathbf{p}_i^t]$, meaning that the frequency feature shift can be represented as $p_s(\mathbf{a}^s, \mathbf{p}^s) \neq p_t(\mathbf{a}^t, \mathbf{p}^t)$.

The issue of disjoint support sets for frequency features.

An appropriate metric to align frequency features between \mathbf{e}_F^s and \mathbf{e}_F^t is challenging to find. Distance measures such as the total variation distance or Kullback-Leibler divergence are not suitable because they are unstable when the supports of distributions are deformed and do not metricize the convergence in law (Feydy et al., 2019), meaning that they do not effectively capture the discrepancy when $\mathbf{e}_{F,i}^s$ and $\mathbf{e}_{F,i}^t$ have disjoint support. The KL divergence, for example, grows unbounded ($KL(\mathbf{e}_{F,i}^s || \mathbf{e}_{F,i}^t) \rightarrow +\infty$) when $\mathbf{e}_{F,i}^s$ and $\mathbf{e}_{F,i}^t$ are far apart, leading to a degradation of alignment and early collapse. An ideal divergence measure could capture the discrepancy even if $\mathbf{e}_{F,i}^s$ and $\mathbf{e}_{F,i}^t$ have disjoint support ($\text{supp}(\mathbf{e}_{F,i}^s) \cap \text{supp}(\mathbf{e}_{F,i}^t) \approx \emptyset$).

The components of frequency features, amplitude \mathbf{a} and phase \mathbf{p} , have different distributions. The phase \mathbf{p} has a uniform distribution over the range of polar angles, which makes it easy to measure the distance between \mathbf{p}_i^s and \mathbf{p}_i^t , bounded in the polar coordinate system $\mathbf{p}_i \in [0, 2\pi)$. However, the amplitude \mathbf{a} has a Rayleigh distribution with an unlimited scale, $\mathbf{a}_i \in [0, +\infty)$, making it difficult to measure the distance between \mathbf{a}_i^s and \mathbf{a}_i^t using the KL divergence. The KL divergence can not provide useful gradients when \mathbf{a}_i^s and \mathbf{a}_i^t are far apart. This leads to a lack of alignment when the amplitudes are far apart, as numerically verified in Figure 5 in the Appendix.

Sinkhorn divergence solves the issue. The Sinkhorn divergence is an entropy-regularized optimal transport distance that enables the comparison of distributions with disjoint supports. Another metric, maximum mean discrepancy (MMD), addresses the issue of disjoint support by considering the geometry of the distributions. However, we demonstrate that MMD has a theoretical weakness that manifests as vanishing gradients or similar artifacts. To address this, RAINCOAT aligns the source features (\mathbf{z}_i^s) and target features (\mathbf{z}_i^t) by minimizing a domain alignment loss based on Sinkhorn. Further details are provided in Appendix A.

5.4. Correction

In this section, we explain how the correction step helps reduce negative transfer by rejecting target unknown samples $\mathbf{x}^t \sim \mathcal{D}^t[\bar{\mathcal{C}}^t]$. The correction step updates the encoder G_{TF} and decoder U_{TF} by solving a reconstruction task on target samples $\mathbf{x}^t \sim \mathcal{D}^t$. This updated G_{TF} repositions the

target features \mathbf{z}_i^t . The target features before and after the correction step are denoted as $\mathbf{z}_{a,i}^t$ and $\mathbf{z}_{c,i}^t$, respectively.

Motivation for reconstructing \mathbf{x}_i^t . The cluster assumption (Chapelle and Zien, 2005) holds that the input data is separated into clusters and that samples within the same cluster have the same label. Based on this, we argue that preserving target discriminative features \mathbf{z}_i^t is important for UniDA, because such features help generate discriminative clusters, including clusters of target unknown samples, which improves UniDA. To do this, RAINCOAT minimizes a reconstruction loss to adapt the feature encoder G_{TF} and decoder U_{TF} . The target features $\mathbf{z}_{a,i}^t$ before the correction step are generated by a shared encoder G_{TF} that aligns the source and target domains. As a result, the target features of common samples $\mathbf{x}^t \sim \mathcal{D}^t[\mathcal{C}^{s,t}]$ should change less in the latent space than those of target unknown samples $\mathbf{x}^t \sim \mathcal{D}^t[\bar{\mathcal{C}}^t]$. This indicates that the corrected encoder G_{TF} maintains the features of common target samples close to their originally assigned label while letting the features of target unknown samples diverge from their originally assigned label. RAINCOAT leverages this to detect and reject target unknown samples, which we discuss next.

5.5. Inference: Detect Target Private Samples

RAINCOAT detects target unknown samples $\mathbf{x}^t \sim \mathcal{D}^t[\bar{\mathcal{C}}^t]$ by determining the movement of target features before and after the correction step. It assumes that when the target domain contains unknown labels, the distribution of the movement will exhibit a bimodal structure.

For brevity, the feature vector \mathbf{z}_i^t is used as an input to H , which consists of prototypes for each class $\mathbf{W} = [\mathbf{w}_1, \mathbf{w}_2, \dots, \mathbf{w}_C]$. Denote the distance (cosine similarity) of \mathbf{z}_i^t to its assigned prototype c as $d(\mathbf{z}_i^t, \mathbf{w}_c)$. Cosine similarity is a reasonable choice because the cross entropy (CE) loss encourages angular separation. It can be interpreted as aligning the feature vectors \mathbf{z}_i^t along its assigned class prototype. The cosine similarity in the form of the dot product gives CE an intrinsic angular property, which is observed in (3) where features naturally separate in the polar coordinates with CE only. Given a target feature \mathbf{z}_i^t and true label $y_i = c$, the cross entropy can be expressed as:

$$\begin{aligned} \mathcal{L}_{CE}(\hat{y}, y) &= -\log \frac{\exp(\mathbf{w}_c^T \mathbf{z}_i^t)}{\sum_j \exp(\mathbf{w}_j^T \mathbf{z}_i^t)} \propto \sum_{j \neq c} \exp(\mathbf{w}_j^T \mathbf{z}_i^t - \mathbf{w}_c^T \mathbf{z}_i^t) \\ &\propto \sum_{j \neq c} \exp(\|\mathbf{z}_i^t\|_2 \|\mathbf{w}_j\|_2 \cos(\theta_j) - \|\mathbf{z}_i^t\|_2 \|\mathbf{w}_c\|_2 \cos(\theta_c)) \end{aligned}$$

As a result, if the target feature \mathbf{z}_i^t is close to its prototypes, then $d(\mathbf{z}_i^t, \mathbf{w}_c)$ will be small, and vice versa. Then RAINCOAT measures the movement by calculating the absolute difference of target features' distance to the assigned prototype before and after correction given by $d_i^{ac} = |d(\mathbf{z}_{a,i}^t, \mathbf{w}_c) - d(\mathbf{z}_{c,i}^t, \mathbf{w}_c)|$.

Algorithm 1 Overview of RAINCOAT

Input: dataset $\mathcal{D}^s, \mathcal{D}^t$; epochs E_1, E_2 ; time-frequency feature encoder, G_{TF} , and decoder, U_{TF} (Alg. 2); prototype classifier H

Stage 1: Alignment (introduced in 5.2, 5.3))

for E_1 epochs **do**

 Extract $\mathbf{z}_i^s, \mathbf{z}_i^t \leftarrow G_{TF}(\mathbf{x}_i^s), G_{TF}(\mathbf{x}_i^t)$

$\mathcal{L}_A \leftarrow \text{SINKHORN}(\mathbf{z}_i^s, \mathbf{z}_i^t)$ (Alg. 3)

$\mathcal{L}_R \leftarrow |\mathbf{x}_i^s - U_{TF}(\mathbf{z}_i^s)|$

$\mathcal{L}_C \leftarrow CE(y_i^s, H(\mathbf{z}_i^s))$

 Update U_{TF}, G_{TF}, H with $\nabla(\mathcal{L}_A + \mathcal{L}_R + \mathcal{L}_C)$

end for

Stage 2: Correction (introduced in 5.4)

Extract features: $\mathbf{z}_{a,i}^t \leftarrow G_{TF}(\mathbf{x}_i^t)$

Distance to prototypes: $\mathbf{d}_{\text{align}} \leftarrow d(\mathbf{z}_{a,i}^t, H)$

for E_2 epochs **do**

$\mathcal{L}_R \leftarrow |\mathbf{x}_i^t - (U_{TF} \circ G_{TF})(\mathbf{x}_i^t)|$

 Update U_{TF}, G_{TF} with $\nabla \mathcal{L}_R$

end for

Extract post-correction: $\mathbf{z}_{c,i}^t \leftarrow G_{TF}(\mathbf{x}_i^t)$

Re-compute: $\mathbf{d}_{\text{correct}} \leftarrow d(\mathbf{z}_{c,i}^t, H)$

Stage 3: Inference (introduced in 5.5)

$d_i^{ac} = |d(\mathbf{z}_{a,i}^t, \mathbf{w}_c) - d(\mathbf{z}_{c,i}^t, \mathbf{w}_c)|$

for c in \mathcal{C}^s **do**

$p \leftarrow \text{Bimodality Test}$

if $p < 0.05$ **then** ▷ Bimodal structure detected

$\mu_c^{\text{common}}, \mu_c^{\text{unknown}} = \text{CLUSTER}(d^{ac} | \hat{y} = c)$

end if

end for

Next, RAINCOAT detects if there are private target samples in each class by first running a bimodality test on each group of \mathcal{C}^s . If the bimodality test tells us d^{ac} has two modalities, it then trains a 2-mean cluster to fit the distribution of d^{ac} . For each class, after we obtain the centroid μ_1, μ_2 , where $\mu_1 < \mu_2$, RAINCOAT takes μ_2 as our threshold to reject ‘‘unknown’’ target samples.

5.6. Overview of RAINCOAT Models

During alignment, RAINCOAT trains a classifier H using labeled source dataset \mathcal{D}^s and a feature encoder G_{TF} and decoder U_{TF} using both \mathcal{D}^s and \mathcal{D}^t . At the same time, it aligns target features \mathbf{z}_i^t with source features \mathbf{z}_i^s using Sinkhorn divergence. The overall loss function in this step has three terms. First, the sinkhorn distance $\mathcal{L}_A(\mathbf{z}_i^t, \mathbf{z}_i^s)$ urges the target features \mathbf{z}_i^t to be aligned with source features \mathbf{z}_i^s . Second, the reconstruction loss $\mathcal{L}_R(\mathbf{x}_i^s, U_{TF}(G_{TF}(\mathbf{x}_i^s)))$ promotes learning of semantic features of \mathcal{D}^s . Third, the classification loss $\mathcal{L}_C(H(G_{TF}(\mathbf{x}_i^s)), y_i^s)$ guides the model to classify samples correctly. In summary, the loss in this step is defined as $\mathcal{L} = \mathcal{L}_A + \mathcal{L}_R + \mathcal{L}_C$.

In this step, target common samples could be classified correctly, and target unknown samples will be misclassified because the G_{TF} aligns all samples without considering the label shift. The correct step aims to correct such negative transfer (target unknown samples) by exploit-

ing target-specific discriminative features by minimizing $\mathcal{L}_R(\mathbf{x}_i^t, U_{TF}(G_{TF}(\mathbf{x}_i^t)))$.

In the inference step, only the trained classifier H and feature encoder G_{TF} before and after correction are utilized. When a target samples \mathbf{x}_i^t to inference is given, RAINCOAT calculates the movement using d_i^{ac} equation followed by a bi-modality test and binary classification (known or unknown) is necessary. An overview of RAINCOAT is in Alg. 1; a detailed overview is in Appendix and Alg. 4.

6. Experiments

6.1. Experimental Setup

Baselines for closed-set DA. We consider 8 closed-set DA methods. For baselines are general unsupervised DA methods: deep correlation alignment (CORAL) (Sun and Saenko, 2016), CDAN (Long et al., 2018b), decision-boundary iterative refinement training with a teacher (DIRT-T) (Shu et al., 2018), and AdaMatch (Berthelot et al., 2022). We also consider four unsupervised DA methods for time series: CODATS (Wilson et al., 2020), adversarial spectral kernel matching for unsupervised time series domain adaptation (AdvSKM) (Liu and Xue, 2021b), and CLUDA (Ozyurt et al., 2022). We additionally consider source-domain-only training (no transfer) implemented by (Ragab et al., 2022). **Baselines for uniDA.** We consider 4 state-of-the-art methods that can reject unknown samples: include UAN (You et al., 2019), DANCE (Saito et al., 2020), OVANet (Saito and Saenko, 2021), and UniOT (Chang et al., 2022). **Datasets.** We consider five benchmark datasets from three distinct problem types: (1) human activity recognition: WISDM (Kwapisz et al., 2011), HAR (Anguita et al., 2013), HHAR (Stisen et al., 2015); (2) mechanical fault detection: Boiler (Shohet et al., 2019); and (3) EEG prediction: Sleep-EDF (Goldberger et al., 2000). Further details on datasets are given in Appendix C.1. **Setup for closed-set DA.** Individual, participant or device IDs define domains in the above datasets. Following existing DA research on time series (Ozyurt et al., 2022; Wilson et al., 2020), we select ten pairs of domains to specify source \mapsto target domains, except for the Boiler dataset where we consider all possible configurations (i.e., 6 scenarios). **Setup for uniDA.** The WISDM dataset is the most challenging because of considerable label shift across participants, e.g., the source participant 29 does not perform the activity ‘jog’ at all, but the target participant 28 performs ‘jog’ 33% of the time. To this end, we consider WISDHM to examine the performance of in-dataset UniDA. In addition, both HHAR and WISDM contain sensor measurements, and they each have one private label (‘bike’ and ‘jog’), making them appropriate for cross-dataset evaluation of UniDA. **Evaluation.** We report accuracy and macro-F1 calculated using target test datasets. Accuracy is computed by dividing the number of correctly classified samples by

the total number of samples. macro-F1 is computed using the unweighted mean of all the per-class F1 scores. It treats all classes equally regardless of their support values. For UniDA, the trade-off between correctly predicting common vs. private classes on the target domain is captured using H-score, defined as the harmonic mean between accuracy on common classes CA_c and accuracy on private classes CA_u , $H\text{-score} = (2CA_c CA_u)/(CA_c + CA_u)$.

6.2. Results

Q1: How effective is RAINCOAT for closed-set DA? Figure 4 shows the average accuracy and standard deviation of each method for selected source-target domain pairs on all datasets. Full results are given in Table 10 (accuracy) and Table 11 (Macro-F1). Overall, RAINCOAT has won 5 out of 5 tests (2 metrics in 5 datasets) and makes an average improvement of accuracy (6.77%) and Macro-F1 (9.00%) over with the strongest baseline across datasets. Specifically, RAINCOAT improves prediction accuracy by 8.65% on HAR, 5.48% on HHAR, 5.8% on WISDM, 2.81% on Sleep-EDF, and 10.43% on Boiler over the strongest baseline on each dataset respectively. In particular, RAINCOAT outperforms CLUDA, the state-of-the-art closed-set DA method for time series, by 8.23% (accuracy) and 10.00% (Macro-F1) averaged over all datasets. RAINCOAT captures and aligns time-frequency features across domains which improves knowledge transfer among time series in the presence of feature shift.

Q2: How effective is RAINCOAT for UniDA? We report the average H-score in Table 1 and the average accuracy results in Appendix 12. Results show that RAINCOAT consistently outperforms baselines and achieves state-of-the-art results on DA for time series under both feature and label shift. We note that changes in features and labels of time series data are different from other types of data such as images, which cause a decrease in the performance of baseline models. However, RAINCOAT has a significant average improvement over the strongest baseline by 16.33% (H-score) across datasets with large gaps. This can be attributed to its time-frequency feature encoder and detecting unknown samples via discriminative features learned using the 'align-and-correct' strategy.

Additional analyses. Next, we study the following questions **Q3:** How effective is the time-frequency encoder? **Q4:** Is Sinkhorn divergence a better measurement for our time-frequency feature? **Q5:** Will the correct step decrease the perform when there is no label shift? We evaluate how relevant the model components are for effective DA. We perform the ablation study using WISDM since it is a more challenging dataset and present results in Table 2. When no component is used (1st row in Table 2), it refers to a source-only model. When Sinkhorn is not used (2nd, 5th row in Table

Table 1. H-score of UniDA using WISDM, WISDM→HHAR, HHAR→WISDM, Shown: mean H-score over 5 independent runs. See Table 12 in Appendix for additional results.

Source → Target	UAN	DANCE	OVANet	UniOT	RAINCOAT
WISDM 3 → 2	0	0	0.07	0.11	0.51
WISDM 3 → 7	0	0	0.2	0.22	0.52
WISDM 13 → 15	0	0.14	0.33	0.36	0.50
WISDM 14 → 19	0.24	0.28	0.31	0.28	0.55
WISDM 27 → 28	0.07	0.07	0.23	0.35	0.59
WISDM 1 → 0	0.41	0.39	0.38	0.40	0.43
WISDM 1 → 3	0.46	0.49	0.45	0.43	0.51
WISDM 10 → 11	0	0	0.34	0.41	0.53
WISDM 22 → 17	0.13	0	0.32	0.41	0.52
WISDM 27 → 15	0.43	0.51	0.46	0.52	0.57
WISDM Avg	0.17	0.19	0.31	0.35	0.52
WISDM Std of Avg	0.04	0.05	0.04	0.05	0.04
<hr/>					
W→H 4 → 0	0	0.14	0.15	0.19	0.49
W→H 5 → 1	0.24	0.22	0.25	0.28	0.53
W→H 6 → 2	0.14	0.12	0.20	0.25	0.55
W→H 7 → 3	0	0.15	0.04	0.14	0.51
W→H 17 → 4	0.35	0.28	0.41	0.45	0.57
W→H 18 → 5	0.20	0.27	0.29	0.32	0.47
W→H 19 → 6	0.19	0.22	0.25	0.28	0.51
W→H 20 → 7	0.11	0.17	0.35	0.41	0.49
W→H 23 → 8	0.21	0.28	0.47	0.51	0.57
W→H Avg	0.16	0.21	0.24	0.28	0.52
W→H Std of Avg	0.03	0.02	0.03	0.02	0.02
<hr/>					
H→W 0 → 4	0.23	0.28	0.33	0.37	0.45
H→W 1 → 5	0.19	0.31	0.38	0.42	0.47
H→W 2 → 6	0.04	0.17	0.23	0.29	0.39
H→W 3 → 7	0.25	0.32	0.34	0.40	0.42
H→W 4 → 17	0.31	0.39	0.41	0.40	0.51
H→W 5 → 18	0.28	0.34	0.37	0.36	0.48
H→W 6 → 19	0.42	0.42	0.46	0.47	0.49
H→W 7 → 20	0.39	0.41	0.41	0.44	0.52
H→W 8 → 23	0.19	0.28	0.32	0.35	0.46
H→W Avg	0.26	0.32	0.36	0.39	0.47
H→W Std of Avg	0.05	0.05	0.03	0.04	0.03

Higher H-score is better. Best performance is indicated in bold.

2), we use MMD to align features. It can be observed that using the frequency encoder alone (2nd row) results in performance improvement (accuracy) of 9.44% for Closed-set DA and 2.33% for UniDA on average. It demonstrates the effectiveness of a frequency encoder for handling the feature shift of time series. By comparing 2nd row with 4th row, we observe Sinkhorn Divergence brings consistent improvement for both Closed-set DA (1.02%) and UniDA (1.11%), which demonstrates the benefit of Sinkhorn Divergence for aligning frequency features. When the frequency encoder (2nd row) is further equipped with a correction step (5th row), it verifies the effectiveness of the correction step when there is a label shift. By comparing the 5th row with the 2nd and 4th row, we find that the correction step does not lead to a performance drop for Closed-set DA. This finding indicates that RAINCOAT is suitable for resolving both feature and label shifts, even if no prior information on feature and label shifts is given.

7. Conclusion

This paper presents a new domain adaptation approach, named RAINCOAT, for time series data. It tackles domain

Domain Adaptation for Time Series Under Feature and Label Shifts

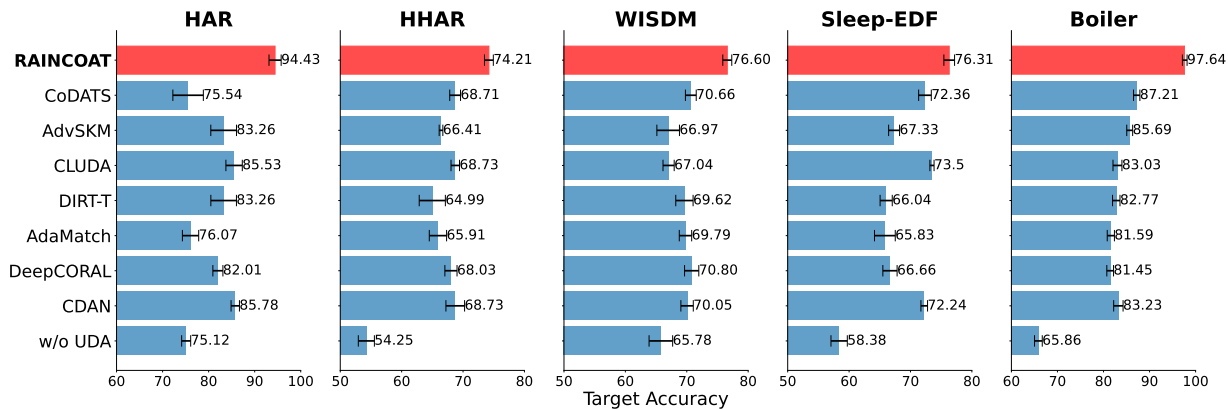


Figure 4. Average performance of multiple Closed-set DA methods across multiple datasets. RAINCOAT consistently outperforms all other methods in accuracy on test sets drawn from the target domain dataset.

Table 2. Ablation analysis of RAINCOAT. Specifically, the frequency encoder, Sinhorn Alignment, and Correct Step modules are shown below. When no component is checked (first row), it refers to the source-only model. We evaluate RAINCOAT on both closed-set and universal DA and also include average accuracy across all 10 scenarios (source \mapsto target domain) on the WISDM dataset.

	Element of RAINCOAT			Closed Set DA				Universal DA					
	Frequency Encoder	Sinhorn	Correct	4 \mapsto 15	7 \mapsto 30	12 \mapsto 17	12 \mapsto 19	Avg (10 scenarios)	1 \mapsto 0	10 \mapsto 11	22 \mapsto 17	27 \mapsto 15	Avg (10 scenarios)
1				79.86	89.32	71.53	54.29	65.78	64.58	54.38	42.98	38.04	40.84
2	✓			89.72	90.12	84.34	83.87	75.22	70.84	65.04	44.81	54.39	42.97
3		✓		82.43	89.88	83.14	76.74	69.66	65.13	57.44	45.14	42.42	41.25
4	✓	✓		95.34	92.36	86.84	84.11	76.24	73.68	72.37	40.79	58.17	44.08
5	✓		✓	90.84	90.01	86.31	79.84	76.04	74.34	66.10	48.01	57.22	46.52
6	✓	✓	✓	97.91	91.28	89.80	85.00	76.60	82.57	76.36	48.16	66.42	53.51

adaptation for time series under both feature and label shifts. By utilizing features from both time and frequency space, aligning them across domains, and correcting misalignments, RAINCOAT enhances transferability and improves label detection. Additionally, RAINCOAT detects label shifts by comparing discriminative features in the target domain. The results from experiments on five datasets show the effectiveness of RAINCOAT, achieving up to 6.77% improvement in closed-set domain adaptation and 16.33% improvement in universal domain adaptation.

Acknowledgements

We gratefully acknowledge the support of the Under Secretary of Defense for Research and Engineering under Air Force Contract No. FA8702-15-D-0001 and awards from NSF under Nos. IIS-2030459 and IIS-2033384, Harvard Data Science Initiative, Amazon Research Award, Bayer Early Excellence in Science Award, AstraZeneca Research, and Roche Alliance with Distinguished Scientists Award. Any opinions, findings, conclusions or recommendations expressed in this material are those of the authors and do not necessarily reflect the views of the funders. The authors declare that there are no conflict of interests.

References

- Suman Ravuri, Karel Lenc, Matthew Willson, Dmitry Kanigin, Remi Lam, Piotr Mirowski, Megan Fitzsimons, Maria Athanassiadou, Sheleem Kashem, Sam Madge, et al. Skilful precipitation nowcasting using deep generative models of radar. *Nature*, 597(7878):672–677, 2021.
- Scott M Lundberg, Bala Nair, Monica S Vavilala, Mayumi Horibe, Michael J Eisses, Trevor Adams, David E Liston, Daniel King-Wai Low, Shu-Fang Newman, Jerry Kim, et al. Explainable machine-learning predictions for the prevention of hypoxaemia during surgery. *Nature Biomedical Engineering*, 2(10):749–760, 2018.
- Xiang Zhang, Ziyuan Zhao, Theodoros Tsiligkaridis, and Marinka Zitnik. Self-supervised contrastive pre-training for time series via time-frequency consistency. In *Advances in Neural Information Processing Systems*, 2022a.
- Xiang Zhang, Marko Zeman, Theodoros Tsiligkaridis, and Marinka Zitnik. Graph-guided network for irregularly sampled multivariate time series. In *International Conference on Learning Representations, ICLR*, 2022b.
- Pang Wei Koh, Shiori Sagawa, Henrik Marklund, Sang Michael Xie, Marvin Zhang, Akshay Balsubramani, Weihua Hu, Michihiro Yasunaga, Richard Lanus Phillips,

- Irena Gao, Tony Lee, Etienne David, Ian Stavness, Wei Guo, Berton A. Earnshaw, Imran S. Haque, Sara Beery, Jure Leskovec, Anshul Kundaje, Emma Pierson, Sergey Levine, Chelsea Finn, and Percy Liang. WILDS: A benchmark of in-the-wild distribution shifts. In *International Conference on Machine Learning (ICML)*, 2021.
- Yawei Luo, Liang Zheng, Tao Guan, Junqing Yu, and Yi Yang. Taking a closer look at domain shift: Category-level adversaries for semantics consistent domain adaptation. *2019 IEEE/CVF Conference on Computer Vision and Pattern Recognition (CVPR)*, pages 2502–2511, 2018.
- Kun Zhang, Bernhard Schölkopf, Krikamol Muandet, and Zhikun Wang. Domain adaptation under target and conditional shift. In *International Conference on Machine Learning*, 2013.
- Yaroslav Ganin, Evgeniya Ustinova, Hana Ajakan, Pascal Germain, Hugo Larochelle, François Laviolette, Mario March, and Victor Lempitsky. Domain-adversarial training of neural networks, 2016.
- Mingsheng Long, Yue Cao, Jianmin Wang, and Michael I. Jordan. Learning transferable features with deep adaptation networks. In *Proceedings of the 32nd International Conference on International Conference on Machine Learning - Volume 37, ICML'15*. JMLR.org, 2015.
- Angela Zhang, Lei Xing, James Zou, and Joseph C Wu. Shifting machine learning for healthcare from development to deployment and from models to data. *Nature Biomedical Engineering*, pages 1–16, 2022c.
- Emily Alsentzer, Michelle M Li, Shilpa N Kobren, Undiagnosed Diseases Network, Isaac S Kohane, and Marinka Zitnik. Deep learning for diagnosing patients with rare genetic diseases. *medRxiv*, pages 2022–12, 2022.
- Sana Tonekaboni, Shalmali Joshi, Melissa D. McCradden, and Anna Goldenberg. What clinicians want: Contextualizing explainable machine learning for clinical end use. In Finale Doshi-Velez, Jim Fackler, Ken Jung, David Kale, Rajesh Ranganath, Byron Wallace, and Jenna Wiens, editors, *Proceedings of the 4th Machine Learning for Healthcare Conference*, volume 106 of *Proceedings of Machine Learning Research*, pages 359–380. PMLR, 09–10 Aug 2019. URL <https://proceedings.mlr.press/v106/tonekaboni19a.html>.
- Robert Geirhos, Jörn-Henrik Jacobsen, Claudio Michaelis, Richard Zemel, Wieland Brendel, Matthias Bethge, and Felix A. Wichmann. Shortcut learning in deep neural networks. *Nature Machine Intelligence*, 2(11):665–673, Nov 2020. ISSN 2522-5839. doi:10.1038/s42256-020-00257-z.
- Alex J. DeGrave, Joseph D. Janizek, and Su-In Lee. Ai for radiographic covid-19 detection selects shortcuts over signal. *Nature Machine Intelligence*, 3(77):610–619, Jul 2021. ISSN 2522-5839. doi:10.1038/s42256-021-00338-7.
- Zachary Chase Lipton, Yu-Xiang Wang, and Alex Smola. Detecting and correcting for label shift with black box predictors. *ArXiv*, abs/1802.03916, 2018.
- Mingsheng Long, Zhangjie Cao, Jianmin Wang, and Michael I Jordan. Conditional adversarial domain adaptation. *Advances in neural information processing systems*, 31, 2018a.
- Guoliang Kang, Lu Jiang, Yi Yang, and Alexander Hauptmann. Contrastive adaptation network for unsupervised domain adaptation. *2019 IEEE/CVF Conference on Computer Vision and Pattern Recognition (CVPR)*, pages 4888–4897, 2019a.
- Kaichao You, Mingsheng Long, Zhangjie Cao, Jianmin Wang, and Michael I. Jordan. Universal domain adaptation. *2019 IEEE/CVF Conference on Computer Vision and Pattern Recognition (CVPR)*, pages 2715–2724, 2019.
- Bo Fu, Zhangjie Cao, Mingsheng Long, and Jianmin Wang. Learning to detect open classes for universal domain adaptation. In *European Conference on Computer Vision*, 2020.
- Yaroslav Ganin and Victor Lempitsky. Unsupervised domain adaptation by backpropagation. In *International conference on machine learning*, pages 1180–1189. PMLR, 2015.
- Ozan Sener, Hyun Oh Song, Ashutosh Saxena, and Silvio Savarese. Learning transferrable representations for unsupervised domain adaptation. *Advances in neural information processing systems*, 29, 2016.
- Yue Zhang, Shun Miao, Tommaso Mansi, and Rui Liao. Task driven generative modeling for unsupervised domain adaptation: Application to x-ray image segmentation. In *International Conference on Medical Image Computing and Computer-Assisted Intervention*, pages 599–607. Springer, 2018.
- Christian S Perone, Pedro Ballester, Rodrigo C Barros, and Julien Cohen-Adad. Unsupervised domain adaptation for medical imaging segmentation with self-ensembling. *NeuroImage*, 194:1–11, 2019.
- Alan Ramponi and Barbara Plank. Neural unsupervised domain adaptation in nlp—a survey. *arXiv preprint arXiv:2006.00632*, 2020.

- Judy Hoffman, Eric Tzeng, Trevor Darrell, and Kate Saenko. Simultaneous deep transfer across domains and tasks. *2015 IEEE International Conference on Computer Vision (ICCV)*, pages 4068–4076, 2015.
- Eric Tzeng, Judy Hoffman, Kate Saenko, and Trevor Darrell. Adversarial discriminative domain adaptation. In *Proceedings of the IEEE conference on computer vision and pattern recognition*, pages 7167–7176, 2017.
- Saeid Motiian, Quinn Jones, Seyed Iranmanesh, and Gianfranco Doretto. Few-shot adversarial domain adaptation. *Advances in neural information processing systems*, 30, 2017.
- Judy Hoffman, Eric Tzeng, Taesung Park, Jun-Yan Zhu, Phillip Isola, Kate Saenko, Alexei Efros, and Trevor Darrell. Cycada: Cycle-consistent adversarial domain adaptation. In *International conference on machine learning*, pages 1989–1998. Pmlr, 2018.
- Artem Rozantsev, Mathieu Salzmann, and Pascal V. Fua. Beyond sharing weights for deep domain adaptation. *IEEE Transactions on Pattern Analysis and Machine Intelligence*, 41:801–814, 2016.
- Baochen Sun and Kate Saenko. Deep coral: Correlation alignment for deep domain adaptation. In *ECCV 2016 Workshops*, 2016.
- Nicolas Courty, Rémi Flamary, Amaury Habrard, and Alain Rakotomamonjy. Joint distribution optimal transportation for domain adaptation. *Advances in Neural Information Processing Systems*, 30, 2017.
- Ievgen Redko, Nicolas Courty, Rémi Flamary, and Devis Tuia. Optimal transport for multi-source domain adaptation under target shift. In *The 22nd International Conference on Artificial Intelligence and Statistics*, pages 849–858. PMLR, 2019.
- Junchi Yan, Xu-Cheng Yin, Weiyao Lin, Cheng Deng, Hongyuan Zha, and Xiaokang Yang. A short survey of recent advances in graph matching. *Proceedings of the 2016 ACM on International Conference on Multimedia Retrieval*, 2016.
- Debasmit Das and C. S. George Lee. Unsupervised domain adaptation using regularized hyper-graph matching. *2018 25th IEEE International Conference on Image Processing (ICIP)*, pages 3758–3762, 2018.
- Guoliang Kang, Lu Jiang, Yi Yang, and Alexander G Hauptmann. Contrastive adaptation network for unsupervised domain adaptation. In *Proceedings of the IEEE/CVF Conference on Computer Vision and Pattern Recognition*, pages 4893–4902, 2019b.
- Ankit Singh. Clda: Contrastive learning for semi-supervised domain adaptation. *Advances in Neural Information Processing Systems*, 34:5089–5101, 2021.
- Shixiang Tang, Peng Su, Dapeng Chen, and Wanli Ouyang. Gradient regularized contrastive learning for continual domain adaptation. In *Proceedings of the AAAI Conference on Artificial Intelligence*, volume 35, pages 2665–2673, 2021.
- Muhammad Ghifary, W Bastiaan Kleijn, Mengjie Zhang, David Balduzzi, and Wen Li. Deep reconstruction-classification networks for unsupervised domain adaptation. In *European conference on computer vision*, pages 597–613. Springer, 2016.
- I-Hong Jhuo, Dong Liu, DT Lee, and Shih-Fu Chang. Robust visual domain adaptation with low-rank reconstruction. In *2012 IEEE conference on computer vision and pattern recognition*, pages 2168–2175. IEEE, 2012.
- Xiaofeng Liu, Chaehwa Yoo, Fangxu Xing, Hyejin Oh, Georges El Fakhri, Je-Won Kang, Jonghye Woo, et al. Deep unsupervised domain adaptation: A review of recent advances and perspectives. *APSIPA Transactions on Signal and Information Processing*, 11(1), 2022.
- S. Purushotham, Wilka Carvalho, Tanachat Nilanon, and Yan Liu. Variational recurrent adversarial deep domain adaptation. In *ICLR*, 2017.
- Garrett Wilson, Janardhan Rao Doppa, and Diane Joyce Cook. Multi-source deep domain adaptation with weak supervision for time-series sensor data. *Proceedings of the 26th ACM SIGKDD International Conference on Knowledge Discovery & Data Mining*, 2020.
- Ruichu Cai, Jiawei Chen, Zijian Li, Wei Chen, Keli Zhang, Junjian Ye, Zhuozhang Li, Xiaoyan Yang, and Zhenjie Zhang. Time series domain adaptation via sparse associative structure alignment. *ArXiv*, abs/2205.03554, 2021.
- Qiao Liu and Hui Xue. Adversarial spectral kernel matching for unsupervised time series domain adaptation. In Zhi-Hua Zhou, editor, *Proceedings of the Thirtieth International Joint Conference on Artificial Intelligence, IJCAI-21*, pages 2744–2750. International Joint Conferences on Artificial Intelligence Organization, 8 2021a.
- Felix Ott, David Rügamer, Lucas Heublein, Bernd Bischl, and Christopher Mutschler. Domain adaptation for time-series classification to mitigate covariate shift. *Proceedings of the 30th ACM International Conference on Multimedia*, 2022.
- Xiaoyong Jin, Youngsuk Park, Danielle Maddix, Hao Wang, and Yuyang Wang. Domain adaptation for time series

- forecasting via attention sharing. In Kamalika Chaudhuri, Stefanie Jegelka, Le Song, Csaba Szepesvari, Gang Niu, and Sivan Sabato, editors, *Proceedings of the 39th International Conference on Machine Learning*, volume 162 of *Proceedings of Machine Learning Research*, pages 10280–10297. PMLR, 17–23 Jul 2022.
- Yilmazcan Ozyurt, Stefan Feuerriegel, and Ce Zhang. Contrastive learning for unsupervised domain adaptation of time series. *ArXiv*, abs/2206.06243, 2022.
- Garrett Wilson, Janardhan Rao Doppa, and Diane J. Cook. Calda: Improving multi-source time series domain adaptation with contrastive adversarial learning, 2021.
- Liang Chen, Yihang Lou, Jianzhong He, Tao Bai, and Min Deng. Evidential neighborhood contrastive learning for universal domain adaptation. In *AAAI Conference on Artificial Intelligence*, 2022a.
- Kuniaki Saito, Donghyun Kim, Stan Sclaroff, and Kate Saenko. Universal domain adaptation through self supervision. *ArXiv*, abs/2002.07953, 2020.
- Guangrui Li, Guoliang Kang, Yi Zhu, Yunchao Wei, and Yi Yang. Domain consensus clustering for universal domain adaptation. *2021 IEEE/CVF Conference on Computer Vision and Pattern Recognition (CVPR)*, pages 9752–9761, 2021a.
- Liang Chen, Qianjin Du, Yihang Lou, Jianzhong He, Tao Bai, and Min Deng. Mutual nearest neighbor contrast and hybrid prototype self-training for universal domain adaptation. In *AAAI*, 2022b.
- Wanxing Chang, Ye Shi, Hoang Duong Tuan, and Jingya Wang. Unified optimal transport framework for universal domain adaptation. *ArXiv*, abs/2210.17067, 2022.
- Shai Ben-David, John Blitzer, Koby Crammer, and Fernando C Pereira. Analysis of representations for domain adaptation. In *NIPS*, 2006.
- Shai Ben-David, John Blitzer, Koby Crammer, Alex Kulesza, Fernando C Pereira, and Jennifer Wortman Vaughan. A theory of learning from different domains. *Machine Learning*, 79:151–175, 2010.
- Jennifer R. Kwapisz, Gary M. Weiss, and Samuel A. Moore. Activity recognition using cell phone accelerometers. *SIGKDD Explor. Newsl.*, 12(2):74–82, mar 2011.
- Zongyi Li, Nikola Borislavov Kovachki, Kamyar Azizzadenesheli, Burigede liu, Kaushik Bhattacharya, Andrew Stuart, and Anima Anandkumar. Fourier neural operator for parametric partial differential equations. In *International Conference on Learning Representations*, 2021b. URL <https://openreview.net/forum?id=c8P9NQVtmnO>.
- F.J. Harris. On the use of windows for harmonic analysis with the discrete fourier transform. *Proceedings of the IEEE*, 66:51–83, 1978.
- J. Feydy, T. Sejourne, F-X. Vialard, S-I. Amari, A. Trouve, and G. Peyre. Interpolating between optimal transport and mmd using sinkhorn divergences. In *AISTATS*, 2019.
- Olivier Chapelle and Alexander Zien. Semi-supervised classification by low density separation. In *International Conference on Artificial Intelligence and Statistics*, 2005.
- Mingsheng Long, ZHANGJIE CAO, Jianmin Wang, and Michael I Jordan. Conditional adversarial domain adaptation. In S. Bengio, H. Wallach, H. Larochelle, K. Grauman, N. Cesa-Bianchi, and R. Garnett, editors, *Advances in Neural Information Processing Systems*, volume 31. Curran Associates, Inc., 2018b.
- Rui Shu, Hung Hai Bui, Hirokazu Narui, and Stefano Ermon. A dirt-t approach to unsupervised domain adaptation. *ArXiv*, abs/1802.08735, 2018.
- David Berthelot, Rebecca Roelofs, Kihyuk Sohn, Nicholas Carlini, and Alexey Kurakin. Adamatch: A unified approach to semi-supervised learning and domain adaptation. In *International Conference on Learning Representations*, 2022. URL <https://openreview.net/forum?id=Q5uh1Nvv5dm>.
- Qiao Liu and Hui Xue. Adversarial spectral kernel matching for unsupervised time series domain adaptation. pages 2744–2750, 08 2021b. doi:10.24963/ijcai.2021/378.
- Mohamed Ragab, Emadeldeen Eldele, Wee Ling Tan, Chuan-Sheng Foo, Zhenghua Chen, Min Wu, Chee Keong Kwoh, and Xiaoli Li. Adatime: A benchmarking suite for domain adaptation on time series data. *arXiv preprint arXiv:2203.08321*, 2022.
- Kuniaki Saito and Kate Saenko. Ovanet: One-vs-all network for universal domain adaptation. *2021 IEEE/CVF International Conference on Computer Vision (ICCV)*, pages 8980–8989, 2021.
- D. Anguita, Alessandro Ghio, L. Oneto, Xavier Parra, and Jorge Luis Reyes-Ortiz. A public domain dataset for human activity recognition using smartphones. In *The European Symposium on Artificial Neural Networks*, 2013.
- Allan Stisen, Henrik Blunck, Sourav Bhattacharya, Thor S. Prentow, Mikkel Baun Kjærgaard, Anind K. Dey, Tobias Sonne, and Mads Møller Jensen. Smart devices are different: Assessing and mitigating mobile sensing heterogeneities for activity recognition. *Proceedings of the 13th ACM Conference on Embedded Networked Sensor Systems*, 2015.

- R. Shohet, M. Kandil, and J.J. McArthur. Simulated boiler data for fault detection and classification, 2019. URL <https://dx.doi.org/10.21227/away-bn36>.
- Ary L. Goldberger, Luis A. Nunes Amaral, L. Glass, Jeffrey M. Hausdorff, Plamen Ch. Ivanov, Roger G. Mark, Joseph E. Mietus, George B. Moody, Chung-Kang Peng, and Harry Eugene Stanley. Physiobank, physiotookit, and physionet: components of a new research resource for complex physiologic signals. *Circulation*, 2000.
- Marco Cuturi. Sinkhorn distances: Lightspeed computation of optimal transport. *Advances in Neural Information Processing Systems*, 26, 2013.
- Marco Cuturi and Gabriel Peyré. A smoothed dual approach for variational wasserstein problems. *SIAM Journal on Imaging Sciences*, 9(1):320–343, 2016.
- Nicolas Fournier and Arnaud Guillin. On the rate of convergence in wasserstein distance of the empirical measure. *Probability Theory and Related Fields*, 162:707–738, 2013.
- Arthur Gretton, Karsten M. Borgwardt, Malte J. Rasch, Bernhard Schölkopf, and Alexander Smola. A kernel two-sample test. *Journal of Machine Learning Research*, 13(25):723–773, 2012. URL <http://jmlr.org/papers/v13/gretton12a.html>.
- A. Genevay, G. Peyre, and M. Cuturi. Learning generative models with sinkhorn divergences. In *AISTATS*, 2018.
- Soheil Kolouri, Phillip E. Pope, Charles E. Martin, and Gustavo K. Rohde. Sliced wasserstein auto-encoders. In *International Conference on Learning Representations*, 2019. URL <https://openreview.net/forum?id=H1xaJn05FQ>.
- James W. Cooley and John W. Tukey. An algorithm for the machine calculation of complex fourier series. *Mathematics of Computation*, 19:297–301, 1965.
- Kamisetty Ramamohan Rao and Pat Yip. *The Transform and Data Compression Handbook*. CRC Press, Inc., USA, 2000. ISBN 0849336929.
- Tian Zhou, Ziqing Ma, Qingsong Wen, Xue Wang, Liang Sun, and Rong Jin. FEDformer: Frequency enhanced decomposed transformer for long-term series forecasting. In *Proceedings of the 39th International Conference on Machine Learning*, volume 162 of *Proceedings of Machine Learning Research*. PMLR, 17–23 Jul 2022.
- Junsik Kim, Tae-Hyun Oh, Seokju Lee, Fei Pan, and In-So Kweon. Variational prototyping-encoder: One-shot learning with prototypical images. *2019 IEEE/CVF Conference on Computer Vision and Pattern Recognition (CVPR)*, pages 9454–9462, 2019.
- Richard Sinkhorn. A relationship between arbitrary positive matrices and doubly stochastic matrices. *Annals of Mathematical Statistics*, 35:876–879, 1964.
- Emadeldeen Eldele, Zhenghua Chen, Chengyu Liu, Min Wu, C. Kwok, Xiaoli Li, and Cuntai Guan. An attention-based deep learning approach for sleep stage classification with single-channel eeg. *IEEE Transactions on Neural Systems and Rehabilitation Engineering*, 29:809–818, 2021.

A. Domain Align of Time-Frequency Feature Cont'd

We first show the distributions of Fourier amplitude and phase.

$$\begin{aligned}
 f(a, p) &= a \times f(x = a \sin p, y = a \cos p) \\
 &= a \times \frac{1}{2\pi} \cdot \exp\left(-\frac{a^2(\sin^2 \theta + \cos^2 \theta)}{2}\right) \\
 &= \frac{a}{2\pi} \cdot \exp\left(-\frac{a^2}{2}\right) \cdot \mathbb{I} \\
 &= a \cdot \exp\left(-\frac{a^2}{2}\right) \cdot \mathbb{I}(a \geq 0) \times \frac{1}{2\pi} \\
 &= \text{Rayleigh}(a | 1) \cdot \text{U}(p | 0, 2\pi) \\
 &\quad (a \geq 0, 0 \leq p \leq 2\pi).
 \end{aligned} \tag{3}$$

We can observe the amplitude can arbitrarily large and thus \mathbf{a}^s and \mathbf{a}^t might have disjoint set when the frequency feature shift is large. As a result, we need to consider a measurement that can measure distance of two arbitrary distributions.

Sinkhorn Divergence. We consider two discrete probability measures represented as sums of weighted Dirac atoms:

$$\boldsymbol{\mu} = \sum_{i=1}^n \mu_i \delta_{\mathbf{z}_i} \text{ and } \boldsymbol{\nu} = \sum_{j=1}^m \nu_j \delta_{\mathbf{z}_j} \tag{4}$$

Here, $\boldsymbol{\mu} \in \mathbb{R}_+^n$ and $\boldsymbol{\nu} \in \mathbb{R}_+^m$ are non-negative vectors of length n and m that sum up to 1. We denote their probabilistic couplings, set Π and cost matrix \mathbf{C} , as:

$$\begin{aligned}
 \Pi(\boldsymbol{\mu}, \boldsymbol{\nu}) &= \{\mathbf{P} \in \mathbb{R}_+^{n \times m}, \mathbf{P}\mathbf{1}_m = \boldsymbol{\mu}, \mathbf{P}^\top \mathbf{1}_n = \boldsymbol{\nu}\} \\
 \mathbf{C} &= (\mathbf{C}_{ij}) \in \mathbb{R}_+^{n \times m}, \mathbf{C}_{ij} = \|\mathbf{z}_i - \mathbf{z}_j\|^p
 \end{aligned} \tag{5}$$

Sinkhorn divergence (Cuturi, 2013; Cuturi and Peyré, 2016) was proposed as an entropic regularization of the Wasserstein distance (Fournier and Guillin, 2013) that interpolates between the pure OT loss for $\eta = 0$ and MMD (Gretton et al., 2012) losses for $\eta \rightarrow \infty$ and offers a computationally efficient way to approximate OT costs. It thus provides a good tradeoff between (a) favorable sample complexity and unbiased gradient estimates, and (b) non-flat geometry of OT (Genevay et al., 2018; Feydy et al., 2019). The Sinkhorn divergence between $\boldsymbol{\mu}$ and $\boldsymbol{\nu}$ is given by

$$\mathcal{S}_\eta(\boldsymbol{\mu}, \boldsymbol{\nu}) = \min_{\mathbf{P} \in \Pi(\boldsymbol{\mu}, \boldsymbol{\nu})} \{(\mathbf{C}, \mathbf{P}) + \eta H(\mathbf{P})\}, \tag{6}$$

where $H(P) = \sum_{i,j} \mathbf{P}_{ij} \log(\mathbf{P}_{ij})$ is the negative entropy and $\eta > 0$ is a regularization parameter. By making η higher, the resulting coupling matrix will be smoother, and as η goes to zero it will be sparser, with the solution being close to that of the original optimal transport problem. The well-known Sinkhorn algorithm for finding such a coupling matrix in an efficient manner is provided in Alg. 3.

Optimal transport losses have appealing geometric properties, but it takes $O(n^3 \log n)$ to compute. On the other hand, discrepancy metrics such as MMD is geometry-aware and can scale up to large batches with a low sample complexity. But we realize that measuring discrepancy of frequency features using Sinkhorn has a stronger Gradient than MMD. Specifically, consider MMD with a RBF kernel, the gradient of MMD w.r.t a particular sample \mathbf{z}^s is $\nabla_{\mathbf{z}^s} D_{MMD}(\mathbf{Z}^s, \mathbf{Z}^t) = \frac{1}{N^2} \sum_j k(\mathbf{z}_i^s, \mathbf{z}_j^s) \frac{\mathbf{z}_j^s - \mathbf{z}_i^s}{\sigma^2} - \frac{2}{NM} \sum_j k(\mathbf{z}_i^s, \mathbf{z}_j^t) \frac{\mathbf{z}_j^t - \mathbf{z}_i^s}{\sigma^2}$. When minimizing MMD, the first term is a repulsive term between the samples from $p(\mathbf{z}^s)$, and the second term is an attractive term between the samples from $p(\mathbf{z}^s)$ and $p(\mathbf{z}^t)$. The L2 norm of the term between two samples \mathbf{z}^s and \mathbf{z}^t is small if $\|\mathbf{z}^s - \mathbf{z}^t\|_2$ is either too small or too large. This is saying if $p(\mathbf{z}^s)$ is far away from $p(\mathbf{z}^t)$, the model will not receive strong gradients (bounded by a small norm). From another viewpoint, (Feydy et al., 2019) demonstrated that the norm of MMD strongly relies on the smoothness of the reference measure and tends to have vanishing gradients when points of the measures' support are disjoint. Now let's look at gradients of Sinkhorn. Denote a Lipschitz cost function as $C(\mathbf{z}^s, \mathbf{z}^t)$. For $\eta > 0$, the associated Gibbs kernel is defined through

$$k_\eta : (\mathbf{z}^s, \mathbf{z}^t) \in \mathcal{Z}^s \times \mathcal{Z}^t \mapsto \exp(-C(\mathbf{z}^s, \mathbf{z}^t)/\eta)$$

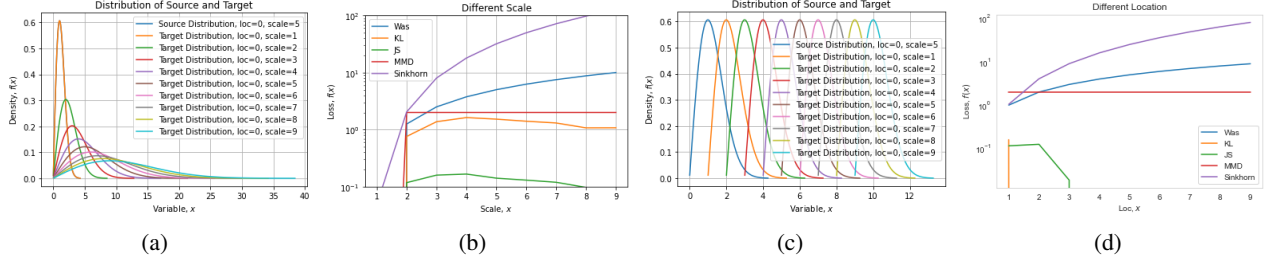


Figure 5. (a) Rayleigh distributions with different scale (b) JSD and KLD (c) Rayleigh distributions with different location (d) JSD and KLD. MSE explode quickly. From b, we can see KL alleviates this problem but it’s still not bounded. From c, we can tell both JS and KL can not provide useful gradients when loc shift is large. It can be problematic when the gap is large and this observation is reasonable because JSD can not provide usable gradients when distributions are supported on non-over-lapping domains. See (Kolouri et al., 2019). Wasserstein distance seems to have a linear relationship to shift, but it’s not bounded as well.

(Feydy et al., 2019) show that the sinkhorn divergence gradient w.r.t a particular sample \mathbf{z}_i^s is largely determined by the magnitude of

$$\eta (\log(\exp(-C(\mathbf{z}_i^s, \mathbf{z}_j^s))/\eta)) - \log(\exp(-C(\mathbf{z}_i^s, \mathbf{z}_j^t)/\eta)))$$

. Different from MMD, the cost function $C(\mathbf{z}^s, \mathbf{z}^t)$ replaces the Euclidean distance with an absolute distance $|\mathbf{z}_i^s - \mathbf{z}_j^t|$. Then, the gradient is always strong regardless of the closeness between \mathbf{z}_i^s and \mathbf{z}_j^t . To numerically verify this claim, we compare the magnitude of the gradients of different shift in Figure 5. It shows Sinkhorn has stronger gradients.

B. Network and Detailed Algorithms

Encoder. What has not yet been emphasized is that practical time series are comprised of a mixture of many (possibly infinite) oscillations at different frequencies. RAINCOAT considers encoding both time and frequency features. We use DFT in our work and leave other approaches for future work. RAINCOAT first smooth input \mathbf{x}_i to prevent frequency leakage by applying a smoothing function. There are many choices of such smoothing functions, but many of the differences are so subtle as to be insignificant in practice. We use the either cosine or Hann window w as a smoothing function (as known as tapering function) formed by using a raised cosine with non-zero endpoints, optimized to minimize the nearest side lobe. It is defined as:

$$w[n] = 0.5 - 0.5 \cos\left(\frac{2\pi n}{N-1}\right) \quad 0 \leq n \leq N-1 \quad (7)$$

After smoothing, DFT is applied on the smoothed \mathbf{x}_i and return \mathbf{v}_i . The DFT implementation in Eq. (1) is inefficient for lengthy signals, and can be scaled up using the fast Fourier transform (FFT) (Cooley and Tukey, 1965). The Fourier domain representation of any real signal satisfies the Hermitian property: $\mathbf{v}[m] = \mathbf{v}[-m]$, meaning that we can save half of the memory by saving a one-sided representation containing only positive frequencies. Complete description of DFT is in Rao and Yip (2000).

Next, RAINCOAT applies a convolution operator on **low frequency modes** of \mathbf{v}_i , which is similar to existing work in neural network based frequency analysis. The intuition behind this is that by acting on low-frequency modes, the operator smooths out high frequency details which tend to be less structured than low frequency components. By doing so, it tends to preserve the low rank structure of signals, which aids alignment. Different from existing works (Li et al., 2021b; Zhou et al., 2022), RAINCOAT does not add a linear transform because this step is used for preserving time space features while RAINCOAT adopts a time feature encoder. Then, we extract the amplitude and phase from the output of the convolution layer as we show that such features (in polar coordinates) are more domain-invariant and inject a useful inductive bias to the model. Last, the extracted frequency features are concatenated with the time features. There are many potential variants such as manifold alignment and self-attention to fuse features from two modalities. We leave it as our future work.

Overall, given a time series \mathbf{x} , the frequency-space feature extraction is conducted as follows. It is first multiplied by (7) to prevent frequency leakage. A convolution is then applied on the smoothed x . Next, the frequency-space feature $e_{\mathcal{F}}$ is obtained by concatenation of results using (2). Regarding the time-space feature extraction, any appropriate network is suitable. We adopt CNN in this work for fair comparison with existing works and demonstrated performance. The

pseudocode for time-frequency feature extraction is presented in Alg. 2

Fourier Neural Operator. Fourier neural operator (FNO) (Li et al., 2021b) perform temporal predictions by combining the Fourier transform with neural networks. Define a convolution operator “*” and weight matrix \mathbf{B} , the Fourier layer in FNO can be summarized as:

$$\begin{aligned} (1) \text{ DFT} & \quad \mathbf{v} = [\text{DFT}(\mathbf{x})] \\ (2) \text{ Frequency Convolution} & \quad \tilde{\mathbf{e}}_{\mathcal{F}} = \mathbf{B} * \mathbf{v} \\ (3) \text{ IDFT} & \quad \tilde{\mathbf{x}} = [\text{IDFT}(\tilde{\mathbf{e}}_{\mathcal{F}})] \end{aligned}$$

FNO then adds the output of the Fourier layer with the bias term (a linear transformation) and applies the activation function. RAINCOAT differs a lot from FNO. The only shared component is the frequency convolution, as we mentioned previously.

Decoder. To learn discriminative features, RAINCOAT learns a decoder through a reconstruction task. We consider a relative simple architecture in this work. Given a latent representation \mathbf{z}_i either from source or target, we split it back to frequency features and time features. Then it is easy to reconstruct \mathbf{x} by perform reconstruction on both $\mathbf{e}_{\mathcal{F}}$ and $\mathbf{e}_{\mathcal{T}}$. We use inverse DFT on $\mathbf{e}_{\mathcal{F}}$ and regular de-convolution network on $\mathbf{e}_{\mathcal{T}}$. Then RAINCOAT adds them together as $\hat{\mathbf{x}}$. We use L1 loss to train the reconstruction task.

Prototypical Classifier. For the classifier H , we adopt a prototypical classifier from (Kim et al., 2019). The normalized feature vector \mathbf{z} is used as an input to H which consists of weight vectors $\mathbf{W} = [\mathbf{w}_1, \mathbf{w}_2, \dots, \mathbf{w}_C]$ where C represents the number of classes. The weight vectors can be regarded as estimated prototypes for each class.

B.1. Detailed Algorithm

In this section, we provide details algorithm for RAINCOAT.

Algorithm 2 Time-Frequency Feature Encoder and Decoder, Domain Alignment via Sinkhorn Divergence

```

1: function TIME-FREQ ENCODER  $G_{\text{TF}}(x)$ 
2:    $x \leftarrow \text{smooth}(x)$ , as shown in (7)
3:    $\mathbf{v}_{\mathcal{F}} \leftarrow \text{DFT}(x)$ 
4:    $\leftarrow \text{SPEC-CONV}(\mathbf{v}_{\mathcal{F}})$ 
5:    $\mathbf{a}, \mathbf{p} \leftarrow \mathbf{v}_{\mathcal{F}}, \text{atan2}(\text{Im}(x_{\mathcal{F}}), \text{Re}(x_{\mathcal{F}}))$ 
6:    $\mathbf{e}_{\mathcal{F}} \leftarrow \text{CONCAT}(\mathbf{a}, \mathbf{p})$ 
7:    $\mathbf{e}_{\mathcal{T}} \leftarrow \text{TIME-CONV}(x)$ 
8:    $\mathbf{z} \leftarrow \text{CONCAT}(\mathbf{e}_{\mathcal{F}}, \mathbf{e}_{\mathcal{T}})$ 
9:   return  $\mathbf{z}$ 
10: end function
11:
12: function TIME-FREQ DECODER  $\mathcal{U}_{\mathcal{T}\mathcal{F}}(z)$ 
13:    $e_{\mathcal{T}}, e_{\mathcal{F}} \leftarrow z$ 
14:    $\bar{x}_{\mathcal{T}}, \bar{x}_{\mathcal{F}} \leftarrow \text{CONVTRANSID}(e_{\mathcal{T}}), \text{IFFT}(e_{\mathcal{F}})$ 
15:    $\bar{x} \leftarrow \bar{x}_{\mathcal{T}} + \bar{x}_{\mathcal{F}}$ ,
16:   return  $\bar{x}$ 
17: end function

```

C. Additional Experimental Results

C.1. Dataset Details

We consider 5 benchmark datasets. (1) **WISDM** (Kwapisz et al., 2011) contains 3-axis accelerometer measurements from 30 participants. The measurements are collected at 20 Hz, and we use non-overlapping segments of 128-time steps to predict the activity (label) of each participant during each time segment. There are 6 labels: walking, jogging, sitting, standing, walking upstairs, and walking downstairs. (2) **Boiler** (Shohet et al., 2019) consists of sensor data from three boilers from 2014/3/24 to 2016/11/30. Each boiler is considered its own domain. The learning task is to detect the mechanical fault of the blowdown valve of each boiler. (3) **HAR** (Anguita et al., 2013) contains measurements of 3-axis accelerometer, 3-axis gyroscope, and 3-axis body acceleration from 30 participants. The measurements are collected at 50 Hz, and we use

Algorithm 3 Simplified illustration of computation of Sinkhorn Divergence (Sinkhorn, 1964)

```

1: function SINKHORN DIVERGENCE( $z^s, z^t$ )
2:    $a, b \leftarrow \mathbf{1}_n/n, \mathbf{1}_n/n$ 
3:    $C \leftarrow \|z^s - z^t\|^p$ 
4:    $K \leftarrow \exp(-C/\eta)$ 
5:   for  $j \leftarrow 1$  to  $J$  do
6:      $\mathbf{a}^{(j)} \leftarrow \boldsymbol{\mu} \oslash K\mathbf{b}^{(j-1)}; \mathbf{b}^{(j)} \leftarrow \boldsymbol{\nu} \oslash K^\top \mathbf{a}^{(j-1)}$ 
7:   end for
8:    $\mathcal{L}_{align} \leftarrow \sum C \text{diag}(\mathbf{a}^{(j)}) K \text{diag}(\mathbf{b}^{(j-1)})$ 
9:   return  $\mathcal{L}_{align}$ 
10: end function
    
```

Method	No. of HP	Threshold
UAN	2	Validated
CMU	3	Validated
USFDA	3	Synthesize unknown samples
ROS	4	Reject 50% of target data
DANCE	3	Decide by No. of classes
OVANet	1	loss function trade off
UniOT	1	partial optimal transport
Ours	0	Radius learned by source

Table 3. Reuse table in OVANet (Saito and Saenko, 2021), Comparison of open-set and universal DA methods. HP denotes hyper-parameter

non-overlapping segments of 128-time steps to classify time series into six activities: walking, walking upstairs, walking downstairs, sitting, standing, and lying down. **(4) HHAR** (Stisen et al., 2015) contains 3-axis accelerometer measurements from 30 participants. The measurements are collected at 50 Hz, and we use non-overlapping segments of 128-time steps to classify time series into six activities: biking, sitting, standing, walking, walking upstairs, and walking downstairs. **(5) Sleep-EDF** (Goldberger et al., 2000) contains electroencephalography (EEG) readings from 20 healthy individuals that are to be classified into five sleep stages: wake (W), non-rapid eye movement stages (N1, N2, N3), and rapid eye movement (REM). Following prior research (Eldele et al., 2021), we perform the analyses using the Fpz-Cz channel. Dataset statistics are in Table 4.

 Table 4. Summary of datasets. Further details about datasets and selected source \mapsto target adaptation scenarios are in Appendix C.2.

Dataset	#Subjects	#Channels	Length	# Class	#Train	# Test
HAR	30	9	128	6	2300	990
HHAR	9	3	128	6	12716	5218
WISDM	30	3	128	6	1350	720
Sleep-EDF	20	1	3000	5	14280	6310
Boiler	3	20	36	2	160719	107400

C.2. Experimental Details

In this section, we provide details on the implementations. We implemented RAINCOAT and all the baseline methods in PyTorch base on here. We run test on a NVIDIA GeForce RTX 3090 graphic card. We implement the time feature extracto via a convolutional network (CNN) (Ragab et al., 2022). This configuration remains the same across all methods so that the difference in prediction performance is attributed to algorithm. When training the model, we use Adam for each method with carefully tuned learning rates for each method. Hyperparamters of Adam are selected after grid search on source test datasets with a range from 1×10^{-4} to $1e - 1$. We report several key hyperparamters in tables 5,6,7,8, and 9. Other hyperparamters are included in the supplementary material. Here, we list several key hyperparameters for RAINCOAT.

Algorithm 4 Detailed overview of RAINCOAT

Input: dataset $\mathcal{D}_s, \mathcal{D}_t$; epochs E_1, E_2

Initialization: Parameter Γ for Time-Frequency Feature Encoder $G_{\mathcal{T}\mathcal{F}}$, Φ for Time-Frequency Feature Decoder $U_{\mathcal{T}\mathcal{F}}$, weight vectors $W = [w_1, w_2, \dots, w_{C^s}]$ for prototypical classifier.

Stage 1: Align, introduced in Section 5.2 5.3

for $e \leftarrow 1$ to E_1 **do**

while \mathcal{D}_t not exhausted **do**

 Sample x^s, y^s from \mathcal{D}_s, x^t from \mathcal{D}_t

 Extract: $z^s \leftarrow G_{\mathcal{T}\mathcal{F}}(x^s)$ (use algorithm 2)

 Extract: $z^t \leftarrow G_{\mathcal{T}\mathcal{F}}(x^t)$ (use algorithm 2)

 Reconstruct $\bar{x}^s \leftarrow U_{\mathcal{T}\mathcal{F}}(z^s)$

 Compute: $\mathcal{L}_{align} = \text{SINKHORN}(z^s, z^t, \epsilon)$

▷ in algorithm 2

 Compute: $\mathcal{L}_{recon} = |x^s - \bar{x}^s|$

 Predict: $\hat{y}_s = \text{CLASSIFIER}(z^s)$

 Compute $\mathcal{L}_{cls} = CE(y^s, \hat{y}_s)$

$\mathcal{L}_{total} = \mathcal{L}_{recon} + \mathcal{L}_{align} + \mathcal{L}_{cls}$

 Update Γ, Φ, W with $\nabla \mathcal{L}_{total}$

end while

end for

Stage 2: Correct, introduced in Sec. 5.4

Compute distance to prototypes before correct:

$$d_{align} = \frac{\mathbf{Z}^s \cdot \mathbf{W}}{\|\mathbf{Z}^s\| \|\mathbf{W}\|}$$

for $e \leftarrow 1$ to E_2 **do**

while \mathcal{D}_t not exhausted **do**

 Sample x^t from \mathcal{D}_t

 Extract: $z^t \leftarrow G_{\mathcal{T}\mathcal{F}}(x^t)$ (use algorithm 2)

 Reconstruct $\bar{x}^t \leftarrow U_{\mathcal{T}\mathcal{F}}(z^t)$

 Compute: $\mathcal{L}_{recon} = |x^s - \bar{x}^s|$

 Update Γ, Φ with $\nabla \mathcal{L}_{recon}$

end while

end for

Compute distance to prototypes after correct:

$$d(\mathbf{Z}, \mathbf{W}) = \frac{\mathbf{Z}^s \cdot \mathbf{W}}{\|\mathbf{Z}^s\| \|\mathbf{W}\|}$$

Stage 3: Inference, introduced in Sec. 5.5

Compute drift during correct:

$$drift = |d_{correct} - d_{align}|$$

for $c \leftarrow 1$ to C **do**

 Compute DIP statistic: $dip = \text{DIP}(\{drift\}_{y=c})$

if $dip < 0.05$ **then**

$$\mu_c^{common}, \mu_c^{private} = \text{K-MEANS}(\{drift\}_{y=c})$$

▷ Two modalities detected

end if

end for

Method	Epoch	Batch Size	Learning rate
CoDATS	50	32	$1e - 3$
AdvSKM	50	32	$5e - 1$
CLUDA	50	32	$1e - 2$
DIRT-T	50	32	$5e - 4$
AdaMatch	50	32	$3e - 3$
DeepCoral	50	32	$5e - 3$
CDAN	50	32	$1e - 2$
RAINCOAT	50	32	$5e - 4$

Table 5. Experimental details for HAR

Hyperparameter	Epoch	Batch Size	Learning rate
CoDATS	50	128	$1e - 2$
AdvSKM	50	128	$5e - 4$
CLUDA	50	128	$5e - 4$
DIRT-T	50	128	$5e - 4$
AdaMatch	50	128	$5e - 4$
DeepCoral	50	128	$5e - 4$
CDAN	50	128	$1e - 3$
RAINCOAT	50	128	$1e - 3$

Table 6. Experimental details for EEG

RAINCOAT uses a Fourier Frequency modes of 64, 200, 64, 64, 10 for HAR, EEG, HHAR, WISDM and Boiler respectively. For the regularization term used in Sinkhorn divergence, we use $1e - 3$ consistently across datasets and experiments.

C.3. Full results of Closed-Set DA

Full tables of results for Closed-Set DA experiments are provided in two separate tables defined by metric: Table 10 shows accuracy scores and Table 11 shows Macro-F1 scores. We can observe that RAINCOAT consistently outperforms baseline across all datasets in terms of two metrics.

C.4. Full results of UniDA

Full tables of results for UniDA experiments are provided in two separate tables defined by metric: Table 12 shows accuracy scores and Table 13 shows H-scores (ref. Sec. 6.1). We can note that accuracy is not an proper metric for evaluating UniDA since it does not reflect the real capability of detecting target unknown samples. It can be high or low due to the class imbalance issue. Overall, RAINCOAT also consistently outperforms baselines for three UniDA settings considered in this work.

Hyperparameter	Epoch	Batch Size	Learning rate
CoDATS	50	64	$1e - 3$
AdvSKM	50	64	$3e - 4$
CLUDA	50	64	$1e - 3$
DIRT-T	50	64	$1e - 3$
AdaMatch	50	64	$2e - 3$
DeepCoral	50	64	$5e - 2$
CDAN	50	64	$1e - 3$
RAINCOAT	50	64	$1e - 3$

Table 7. Experimental details for WISDM

Hyperparameter	Epoch	Batch Size	Learning rate
CoDATS	50	32	$1e-3$
AdvSKM	50	32	$3e-4$
CLUDA	50	32	$1e-3$
DIRT-T	50	32	$1e-3$
AdaMatch	50	32	$3e-3$
DeepCoral	50	32	$5e-4$
CDAN	50	32	$1e-3$
RAINCOAT	50	32	$1e-3$

Table 8. Experimental details for HHAR

Hyperparameter	Epoch	Batch Size	Learning rate
CoDATS	30	32	$5e-4$
AdvSKM	30	32	$1e-3$
CLUDA	30	32	$1e-3$
DIRT-T	30	32	$1e-3$
AdaMatch	30	32	$3e-3$
DeepCoral	30	32	$5e-4$
CDAN	30	32	$1e-3$
RAINCOAT	50	32	$1e-3$

Table 9. Experimental details for Boiler

Domain Adaptation for Time Series Under Feature and Label Shifts

Table 10. Prediction accuracy for each dataset between various subjects. Shown: mean Accuracy over 5 independent runs.

Sour \mapsto Tar	w/o UDA	CDAN	DeepCORAL	AdaMatch	DIRT-T	CLUDA	AdvSKM	CoDATS	RAINCOAT
HAR 2 \mapsto 11	76.56	85.42	90.63	75.00	80.21	81.77	98.96	68.23	100
HAR 6 \mapsto 23	67.36	87.50	84.38	80.20	74.31	92.01	88.54	74.31	95.83
HAR 7 \mapsto 13	83.68	92.01	87.50	85.76	82.99	99.31	92.71	77.43	100
HAR 9 \mapsto 18	24.65	58.86	46.88	56.59	59.03	67.71	74.65	63.89	75.69
HAR 12 \mapsto 16	61.11	66.67	65.28	49.65	67.01	65.28	69.44	66.32	86.52
HAR 13 \mapsto 19	88.89	96.52	95.49	94.79	99.30	94.44	93.05	94.09	100
HAR 18 \mapsto 21	100	100	100	100	98.61	98.96	100	99.65	100
HAR 20 \mapsto 6	94.10	95.13	95.49	84.37	92.36	97.22	85.41	70.49	93.41
HAR 23 \mapsto 13	71.18	82.64	69.79	68.75	74.72	72.92	79.51	56.25	86.52
HAR 24 \mapsto 12	83.68	93.40	87.50	70.83	94.27	99.31	96.87	82.81	93.75
HAR Avg	75.12	85.78	82.01	76.07	83.26	85.53	83.26	75.54	94.43
HAR Std of Avg	0.98	0.91	1.09	1.77	2.78	1.78	2.79	3.31	1.32
HHAR 0 \mapsto 2	64.51	76.19	84.23	84.78	77.83	79.84	78.94	79.61	87.72
HHAR 1 \mapsto 6	70.63	92.57	90.14	92.31	88.54	93.40	87.91	90.90	93.33
HHAR 2 \mapsto 4	45.42	52.57	47.08	54.50	50.69	45.90	52.57	60.07	63.75
HHAR 4 \mapsto 0	32.81	29.09	28.13	36.45	32.22	38.84	33.49	21.80	46.46
HHAR 4 \mapsto 5	78.32	97.27	90.49	78.45	93.16	94.08	92.64	97.66	98.05
HHAR 5 \mapsto 1	90.63	96.16	89.91	94.20	91.86	95.57	92.71	97.66	98.25
HHAR 5 \mapsto 2	25.67	35.04	38.39	41.96	38.62	33.93	36.53	41.44	42.63
HHAR 7 \mapsto 2	32.37	37.05	34.45	37.65	38.10	37.80	39.95	38.54	43.32
HHAR 7 \mapsto 5	39.26	75.26	55.73	63.80	72.46	75.26	65.49	58.15	84.17
HHAR 8 \mapsto 4	62.92	96.11	76.88	64.69	65.83	96.11	83.75	97.01	93.75
HHAR Avg	54.25	68.73	68.03	65.91	64.99	68.73	66.41	68.71	74.21
HHAR Std of Avg	1.31	1.52	0.99	1.41	2.13	0.69	0.30	0.88	0.72
WISDM 2 \mapsto 32	81.16	89.37	87.92	74.39	77.78	73.91	70.83	77.29	79.71
WISDM 4 \mapsto 15	79.86	65.97	62.50	78.47	70.83	67.36	95.85	70.83	95.85
WISDM 7 \mapsto 30	89.32	84.79	91.26	89.64	90.61	86.40	93.85	83.20	91.28
WISDM 12 \mapsto 17	71.53	70.48	79.86	73.26	70.20	65.97	77.08	70.17	89.80
WISDM 12 \mapsto 19	54.29	51.01	51.77	55.30	51.51	49.24	47.47	47.47	85.00
WISDM 18 \mapsto 20	83.74	88.62	64.23	75.20	85.36	83.74	81.30	76.01	92.23
WISDM 20 \mapsto 30	67.96	77.02	81.88	74.76	71.84	72.49	21.28	82.85	91.66
WISDM 21 \mapsto 31	21.29	46.58	54.62	31.32	54.41	49.97	44.45	52.61	59.09
WISDM 25 \mapsto 29	26.11	44.33	53.89	57.78	60.04	35.00	74.79	53.89	82.97
WISDM 26 \mapsto 2	82.52	83.33	77.44	87.20	66.46	86.47	74.95	83.29	83.50
WISDM Avg	65.78	70.05	70.80	69.79	69.62	67.04	66.97	70.66	76.60
WISDM Std of Avg	1.92	1.01	1.16	1.01	1.41	0.91	1.84	0.88	0.73
Sleep-EDF 0 \mapsto 11	55.60	68.94	57.22	63.86	65.88	57.87	56.51	69.53	74.41
Sleep-EDF 2 \mapsto 5	60.03	69.53	60.41	72.39	72.85	71.86	65.62	71.83	73.76
Sleep-EDF 12 \mapsto 5	72.01	78.45	75.00	72.09	78.97	79.39	76.49	79.28	79.81
Sleep-EDF 7 \mapsto 18	53.91	73.18	65.82	71.61	74.34	74.49	60.93	73.19	75.32
Sleep-EDF 16 \mapsto 1	40.21	74.53	69.53	57.86	81.82	75.83	72.96	75.32	78.64
Sleep-EDF 9 \mapsto 14	75.00	80.14	82.22	82.55	86.14	86.32	76.75	81.64	87.17
Sleep-EDF 4 \mapsto 12	48.76	67.08	64.97	48.17	68.48	66.53	66.14	71.68	69.86
Sleep-EDF 10 \mapsto 7	67.86	74.35	76.05	60.41	75.05	75.23	74.31	73.31	77.23
Sleep-EDF 6 \mapsto 3	75.20	80.99	78.38	78.12	83.66	81.96	78.90	83.59	84.58
Sleep-EDF 8 \mapsto 10	35.21	55.16	36.79	51.25	46.01	65.70	44.76	44.22	62.35
Sleep-EDF Avg	58.38	72.24	66.66	65.83	66.04	73.50	67.33	72.36	76.31
Sleep-EDF Std of Avg	1.33	0.54	1.16	1.69	0.99	0.34	0.89	1.03	0.87
Boiler 1 \mapsto 2	57.09	67.93	67.13	67.42	68.13	68.93	72.43	75.74	98.06
Boiler 1 \mapsto 3	74.54	94.98	93.32	94.02	94.88	95.36	96.14	97.32	99.57
Boiler 2 \mapsto 1	73.14	85.96	84.32	84.32	87.76	88.74	89.32	90.23	97.33
Boiler 2 \mapsto 3	66.09	93.32	91.53	92.89	92.62	91.31	91.53	92.89	93.18
Boiler 3 \mapsto 1	74.99	93.89	92.43	93.01	93.14	93.92	94.77	95.32	98.1
Boiler 3 \mapsto 2	61.31	63.32	60.39	57.93	60.43	60.43	70.62	72.32	99.57
Boiler Avg	65.86	83.23	81.45	81.59	82.77	83.03	85.69	87.21	97.64
Boiler Std of Avg	0.84	1.02	0.73	0.78	0.81	0.97	0.64	0.69	0.51

Higher is better. Best value in bold.

Domain Adaptation for Time Series Under Feature and Label Shifts

Table 11. Macro-F1 for each dataset between various subjects. Shown: mean Accuracy over 5 independent runs.

Sour \mapsto Tar	w/o UDA	CDAN	DeepCORAL	AdaMatch	DIRT-T	CLUDA	AdvSKM	CoDATS	RAINCOAT
HAR 2 \mapsto 11	0.69	0.85	0.91	0.73	0.81	0.81	0.99	0.66	1.00
HAR 6 \mapsto 23	0.63	0.88	0.81	0.81	0.68	0.92	0.87	0.71	0.96
HAR 7 \mapsto 13	0.84	0.91	0.87	0.86	0.82	0.99	0.92	0.78	1.00
HAR 9 \mapsto 18	0.17	0.61	0.44	0.55	0.58	0.67	0.73	0.60	0.76
HAR 12 \mapsto 16	0.58	0.64	0.65	0.48	0.62	0.64	0.68	0.64	0.86
HAR 13 \mapsto 19	0.91	0.97	0.95	0.94	0.99	0.94	0.93	0.93	1.00
HAR 18 \mapsto 21	1.00	1.00	1.00	1.00	0.98	0.99	1.00	0.99	1.00
HAR 20 \mapsto 6	0.94	0.95	0.95	0.84	0.92	0.98	0.84	0.65	0.94
HAR 23 \mapsto 13	0.71	0.82	0.70	0.67	0.74	0.71	0.77	0.54	0.86
HAR 24 \mapsto 12	0.84	0.92	0.88	0.70	0.93	0.99	0.96	0.81	0.94
HAR Avg	0.73	0.86	0.82	0.76	0.81	0.86	0.87	0.72	0.93
HAR Std of Avg	0.024	0.014	0.015	0.011	0.032	0.005	0.010	0.04	0.005
HHAR 0 \mapsto 2	0.60	0.70	0.86	0.83	0.76	0.82	0.72	0.73	0.87
HHAR 1 \mapsto 6	0.64	0.93	0.91	0.93	0.86	0.94	0.88	0.90	0.93
HHAR 2 \mapsto 4	0.32	0.52	0.45	0.46	0.51	0.44	0.44	0.46	0.59
HHAR 4 \mapsto 0	0.29	0.27	0.26	0.32	0.30	0.40	0.33	0.20	0.45
HHAR 4 \mapsto 5	0.78	0.98	0.90	0.76	0.93	0.94	0.93	0.96	0.98
HHAR 5 \mapsto 1	0.90	0.98	0.90	0.94	0.90	0.96	0.92	0.94	0.98
HHAR 5 \mapsto 2	0.19	0.35	0.36	0.40	0.36	0.37	0.35	0.41	0.41
HHAR 7 \mapsto 2	0.31	0.32	0.32	0.37	0.34	0.36	0.41	0.36	0.44
HHAR 7 \mapsto 5	0.36	0.76	0.50	0.60	0.73	0.65	0.64	0.59	0.86
HHAR 8 \mapsto 4	0.58	0.97	0.73	0.61	0.64	0.84	0.83	0.95	0.94
HHAR Avg	0.5	0.68	0.62	0.62	0.64	0.67	0.65	0.63	0.75
HHAR Std of Avg	0.022	0.013	0.007	0.013	0.023	0.008	0.003	0.006	0.004
WISDM 2 \mapsto 32	0.68	0.72	0.71	0.59	0.65	0.64	0.61	0.66	0.68
WISDM 4 \mapsto 15	0.52	0.44	0.42	0.54	0.41	0.61	0.55	0.41	0.98
WISDM 7 \mapsto 30	0.77	0.70	0.85	0.76	0.78	0.81	0.84	0.75	0.86
WISDM 12 \mapsto 17	0.53	0.50	0.67	0.67	0.56	0.59	0.53	0.62	0.72
WISDM 12 \mapsto 19	0.36	0.31	0.35	0.38	0.39	0.41	0.35	0.37	0.78
WISDM 18 \mapsto 20	0.81	0.87	0.63	0.66	0.67	0.70	0.71	0.76	0.92
WISDM 20 \mapsto 30	0.56	0.64	0.67	0.54	0.65	0.70	0.61	0.72	0.87
WISDM 21 \mapsto 31	0.10	0.31	0.27	0.16	0.28	0.27	0.28	0.30	0.43
WISDM 25 \mapsto 29	0.15	0.23	0.25	0.24	0.21	0.26	0.28	0.30	0.44
WISDM 26 \mapsto 2	0.69	0.71	0.64	0.74	0.54	0.75	0.55	0.70	0.75
WISDM Avg	0.52	0.54	0.52	0.54	0.54	0.57	0.55	0.56	0.74
WISDM Std of Avg	0.031	0.020	0.006	0.015	0.012	0.029	0.013	0.014	0.010
Sleep-EDF 0 \mapsto 11	0.48	0.54	0.50	0.52	0.53	0.47	0.48	0.50	0.54
Sleep-EDF 2 \mapsto 5	0.47	0.62	0.53	0.62	0.63	0.66	0.59	0.53	0.65
Sleep-EDF 12 \mapsto 5	0.59	0.68	0.65	0.66	0.67	0.69	0.64	0.66	0.70
Sleep-EDF 7 \mapsto 18	0.53	0.69	0.62	0.59	0.71	0.71	0.60	0.61	0.72
Sleep-EDF 16 \mapsto 1	0.43	0.62	0.58	0.48	0.66	0.67	0.63	0.58	0.70
Sleep-EDF 9 \mapsto 14	0.61	0.68	0.71	0.67	0.75	0.72	0.68	0.71	0.76
Sleep-EDF 4 \mapsto 12	0.42	0.59	0.59	0.37	0.59	0.55	0.59	0.58	0.62
Sleep-EDF 10 \mapsto 7	0.58	0.67	0.72	0.37	0.68	0.71	0.72	0.71	0.73
Sleep-EDF 6 \mapsto 3	0.67	0.73	0.70	0.62	0.75	0.73	0.72	0.70	0.75
Sleep-EDF 8 \mapsto 10	0.41	0.43	0.36	0.46	0.39	0.65	0.46	0.38	0.61
Sleep-EDF Avg	0.52	0.63	0.60	0.54	0.64	0.65	0.61	0.60	0.68
Sleep-EDF Std of Avg	0.026	0.005	0.015	0.004	0.005	0.007	0.003	0.012	0.008
Boiler 1 \mapsto 2	0.52	0.63	0.63	0.64	0.65	0.68	0.73	0.73	0.98
Boiler 1 \mapsto 3	0.74	0.95	0.93	0.94	0.95	0.95	0.96	0.97	0.98
Boiler 2 \mapsto 1	0.70	0.81	0.83	0.83	0.85	0.86	0.88	0.91	0.97
Boiler 2 \mapsto 3	0.60	0.91	0.90	0.91	0.91	0.90	0.90	0.91	0.91
Boiler 3 \mapsto 1	0.70	0.94	0.90	0.93	0.92	0.94	0.94	0.95	0.97
Boiler 3 \mapsto 2	0.55	0.59	0.60	0.54	0.61	0.58	0.69	0.70	0.99
Boiler Avg	0.635	0.80	0.80	0.80	0.82	0.82	0.85	0.86	0.97
Boiler Std of Avg	0.008	0.010	0.007	0.008	0.010	0.006	0.007	0.005	0.005

Higher is better. Best value in bold.

Table 12. Accuracy of UniDA using WISDM, WISDM→HHAR, HHAR→WISDM, Shown: mean Accuracy over 5 independent runs. Closed-Set DA baselines are colored in blue.

Source → Target	No. Target Private Class	CLUDA	UAN	DANCE	OVANet	UniOT	RAINCOAT (A)	RAINCOAT (with A&C)
WISDM 3 → 2	1	31.71	8.04	8.53	25.61	26.78	28.05	28.05
WISDM 3 → 7	1	23.96	8.19	8.33	34.38	30.31	25.92	25.92
WISDM 13 → 15	2	54.58	9.85	14.58	10.42	16.46	58.33	64.58
WISDM 14 → 19	2	30.30	39.03	44.00	42.42	40.32	46.21	53.78
WISDM 27 → 28	2	8.98	6.94	6.74	7.87	10.98	22.92	53.70
WISDM 1 → 0	2	71.05	70.34	75.71	74.29	73.14	73.68	82.57
WISDM 1 → 3	3	0.00	32.85	38.46	61.54	36.31	11.54	35.54
WISDM 10 → 11	4	60.52	31.80	30.26	35.53	39.35	72.37	76.36
WISDM 22 → 17	4	26.32	27.87	23.68	40.79	38.31	40.79	48.16
WISDM 27 → 15	4	56.25	22.18	27.08	60.42	52.34	58.17	66.42
WISDM Avg		36.37	25.71	27.70	33.28	36.43	44.08	53.51
WISDM Std of Avg		1.05	2.09	1.95	0.97	1.25	1.06	1.41
W → H 4 → 0	1	32.43	24.5	30.73	35.24	36.51	34.32	44.14
W → H 5 → 1	1	20.32	31.0	15.32	26.31	28.14	27.94	35.65
W → H 6 → 2	1	60.32	34.7	32.32	40.35	48.94	65.12	69.01
W → H 7 → 3	1	51.84	21.10	36.84	39.46	50.35	55.10	60.88
W → H 17 → 4	1	12.31	24.50	15.94	25.31	26.32	24.98	28.41
W → H 18 → 5	1	35.85	26.60	29.65	36.14	33.46	35.70	40.76
W → H 19 → 6	1	46.39	32.75	38.13	47.98	49.32	50.17	54.76
W → H 20 → 7	1	62.32	39.83	42.90	58.11	60.31	64.98	64.98
W → H 23 → 8	1	53.76	32.71	40.87	58.32	52.47	60.71	62.84
W → H Avg		37.55	29.74	39.06	40.80	42.87	46.55	51.35
W → H Std of Avg		1.04	1.38	1.98	1.65	1.74	1.31	1.22
H → W 0 → 4	1	59.32	55.30	61.94	63.14	64.07	62.98	64.84
H → W 1 → 5	1	56.17	50.33	58.10	60.14	61.46	60.94	62.85
H → W 2 → 6	1	50.44	49.85	52.51	54.84	56.15	55.95	57.11
H → W 3 → 7	1	52.21	53.01	55.91	55.71	58.91	56.42	60.95
H → W 4 → 17	1	39.87	37.04	41.39	41.01	42.50	41.94	44.95
H → W 5 → 18	1	47.72	47.80	50.35	51.87	52.22	49.95	51.27
H → W 6 → 19	1	44.50	43.09	46.19	44.08	45.93	46.05	51.86
H → W 7 → 20	1	50.92	54.01	59.85	61.35	61.06	47.00	62.59
H → W 8 → 23	1	44.50	42.06	43.66	48.14	49.71	47.77	52.64
H → W Avg		44.47	48.05	52.22	53.36	54.67	52.11	56.57
H → W Std of Avg		1.31	1.39	1.21	0.94	1.05	0.97	1.08

Higher Accuracy is better. Best value in bold.

Table 13. H-Score of UniDA using WISDM, WISDM→HHAR, HHAR→WISDM, Shown: mean Accuracy over 5 independent runs.

Sour \mapsto Tar	No. Tar Private Class	UAN	DANCE	OVANet	UniOT	RAINCOAT
WISDM 3 \mapsto 2	1	0	0	0.07	0.11	0.51
WISDM 3 \mapsto 7	1	0	0	0.2	0.22	0.52
WISDM 13 \mapsto 15	2	0	0.14	0.33	0.36	0.50
WISDM 14 \mapsto 19	2	0.24	0.28	0.31	0.28	0.55
WISDM 27 \mapsto 28	2	0.07	0.07	0.23	0.35	0.59
WISDM 1 \mapsto 0	2	0.41	0.39	0.38	0.40	0.43
WISDM 1 \mapsto 3	3	0.46	0.49	0.45	0.43	0.51
WISDM 10 \mapsto 11	4	0	0	0.34	0.41	0.53
WISDM 22 \mapsto 17	4	0.13	0	0.32	0.41	0.52
WISDM 27 \mapsto 15	4	0.43	0.51	0.46	0.52	0.57
WISDM Avg		0.17	0.19	0.31	0.35	0.52
WISDM Std of Avg		0.04	0.05	0.04	0.05	0.04
W→H 4 \mapsto 0	1	0	0.14	0.15	0.19	0.49
W→H 5 \mapsto 1	1	0.24	0.22	0.25	0.28	0.53
W→H 6 \mapsto 2	1	0.14	0.12	0.20	0.25	0.55
W→H 7 \mapsto 3	1	0	0.15	0.04	0.14	0.51
W→H 17 \mapsto 4	1	0.35	0.28	0.41	0.45	0.57
W→H 18 \mapsto 5	1	0.20	0.27	0.29	0.32	0.47
W→H 19 \mapsto 6	1	0.19	0.22	0.25	0.28	0.51
W→H 20 \mapsto 7	1	0.11	0.17	0.35	0.41	0.49
W→H 23 \mapsto 8	1	0.21	0.28	0.47	0.51	0.57
W→H Avg		0.16	0.21	0.24	0.28	0.52
W→H Std of Avg		0.03	0.02	0.03	0.02	0.02
H→W 0 \mapsto 4	1	0.23	0.28	0.33	0.37	0.45
H→W 1 \mapsto 5	1	0.19	0.31	0.38	0.42	0.47
H→W 2 \mapsto 6	1	0.04	0.17	0.23	0.29	0.39
H→W 3 \mapsto 7	1	0.25	0.32	0.34	0.40	0.42
H→W 4 \mapsto 17	1	0.31	0.39	0.41	0.40	0.51
H→W 5 \mapsto 18	1	0.28	0.34	0.37	0.36	0.48
H→W 6 \mapsto 19	1	0.42	0.42	0.46	0.47	0.49
H→W 7 \mapsto 20	1	0.39	0.41	0.41	0.44	0.52
H→W 8 \mapsto 23	1	0.19	0.28	0.32	0.35	0.46
H→W Avg		0.26	0.32	0.36	0.39	0.47
H→W Std of Avg		0.05	0.05	0.03	0.04	0.03

Higher H-Score is better. Best value in bold.